This is to certify that the

thesis entitled

FREQUENCY DOMAIN FEATURES OF BACKSCATTERED ACOUSTIC RADIATION FROM BIOLOGICAL TISSUE

presented by

CHARLES JOSEPH deSOSTOA

has been accepted towards fulfillment
of the requirements for

M.S. degree in Electrical Eng. & Sys. Sci.

Don Reinhard

Major professor

Date 4/11/79

FREQUENCY DOMAIN FEATURES OF BACKSCATTERED ACOUSTIC RADIATION FROM BIOLOGICAL TISSUE

By

Charles Joseph deSostoa

A THESIS

Submitted to

Michigan State University
in partial fulfillment of the requirements
for the degree of

MASTER OF SCIENCE

Department of Electrical Engineering
and Systems Science

1979

ABSTRACT

FREQUENCY DOMAIN FEATURES OF BACKSCATTERED ACOUSTIC RADIATION FROM BIOLOGICAL TISSUE

By

Charles Joseph deSostoa

This thesis represents a preliminary investigation into the feasibility of indentifying tissue types based on spectral properties of ultrasound echoes. Toward this end, diffuse ultrasound echoes from in vivo human liver and spleen were investigated in order to develop spectral tissue signatures for these organs. The interrogation was performed by a broadbanded 1 MHz transducer operated in the pulse/echo mode. A 5 MHz sampling rate was used to digitize the backscattered signal and the digital data was stored onto magnetic tape for postprocessing. The postprocessing of data collected consisted of the following two procedures; first, Fourier Transformation of the digitized waveforms, and second, calculation of statistical measures of the spectra. Various combinations of these statistical measures were studied in order to assist in tissue classification. The two classifiers investigated were the scatter plot method and minimum Mahalanobis distance method. Data generated from a single subject as well as from a group of 5 subjects was used for testing the two

classification methods. For the scatter plot method and two dimensional feature space, succesful classification rates of 0.73 and 0.83 were achieveable for group and individual data sets respectively. Applying the Mahalanobis method to the group of 5 subjects yielded success rates ranging from 0.72 to 0.79 for the more successful combinations of features. Attenuation factors have been applied to the backscattered spectra to correct for overlying tissue effects. A slight increase in the effectiveness of the features to facilitate tissue classification was observed and indicates that more exact methods for applying attenuation correction factors could prove useful.

TO MADELYN AND X

ACKNOWLEDGMENTS

The author extends his greatest gratitude to Dr. D. K. Reinhard, his thesis advisor, who has been a constant source of guidance and support. Sincere appreciation is expressed to Dr. G. I. Harris and Mr. D. A. Gift for their valued advice. Appreciation is also expressed to Dr. R. Nettleton, a member of the guidance committee, for his review of and suggestions to this thesis.

A very special thanks is extended to Dr. H. R. Zapp for his extensive review of this thesis and numerous suggestions during the course of this research.

Additional thanks are expressed to Dr. T. Adams, Mr. M. Steinmetz, and Mr. B. Johnston for their help and support.

TABLE OF CONTENTS

LIST OF TABLES

LIST OF FIGURES

CHAPTER I

INTRODUCTION

In recent years much research has been conducted in the field of biomedical ultrasonics. In particular, considerable interest and effort has been directed toward quantifying the interaction between various ultrasonic interrogation beams and certain biological tissues. The ultimate goal of such studies is the determination of a set of quantifying features that would enable the researcher to discriminate between normal and pathological states of a given tissue. The investigation of quantifying features, commonly referred to as signatures, includes signal amplitude analysis, impediography, time delay spectroscopy, investigation of frequency dependent absorption, and frequency and angle dependent scattering. The above techniques represent only a cross-section of those developed to date, rather than a comprehensive list.

This thesis investigates properties of the spectral energy distribution of ultrasound backscattered from biological tissue. First, a brief examination of the basic nature by which sound energy propagates and is scattered will be presented. Second, a mathematical model for both the interaction of ultrasound radiation with tissue and the effects of overlying tissue on this model will be discussed. The model is applied to idealized scatters including point, cylinder, and plane sources. Finally, classification of samples will be performed using feature spaces defined by subsets of eight statistical measures determined from the tissue spectra. The effects of overlying

tissue will be noted on the ability of the classifier to interpret the information correctly. Two different biological tissues were studied experimentally, namely; human liver, and human spleen.

1.1 PREVIOUS WORK

In recent years a variety of advanced techniques designed to extract information about the acoustical properties of soft-tissue structures have been investigated. Of these techniques, those employing frequency domain analysis have received much attention and have proven successful in the differentiation of certain tissue states.

Lele, et al.[1] have demonstrated tissue pathology discrimination by considering the state dependence of the attenuation coefficient. Comparing the backscattered frequency spectrum of a known reflector (i.e. glass plate) with and without intervening tissue, they observed an alteration of the spectral energy distribution. It was noted that different tissue states demonstrated detectable changes in the attenuation coefficient as a function of frequency. Lele[1] has investigated this phenomenon for skeletal muscle with localized areas of heat necrotization and infarction by vascular occlusion and from *in vitro* experiments on specimens of normal myocardium and anemic infarcts. In addition, Lizzi, et al.[2,3,4] have demonstrated the pathology frequency dependence of the attenuation coefficient for vitrious hemorraging of the eye *in vivo*. Results from both studies have proven to be relatively successful in determining tissue state differentiation features.

Lizzi[3] has also observed spectrum shaping due to pathologies characteristic of well defined, thin membranes. More specifically,

it was noted that the frequency domain of an acoustic pulse scattered from a detached retina exhibited a scalloped spectrum. The scalloped form was due to the destructive interference between reflections from the anterior and posterior surfaces.

Cepstral signal processing of reflected acoustic waves from tissue structures has been investigated by Fraser, Birnholtz, and Kino[5]. The cepstra corresponds to the Fourier transformed log power spectrum of a signal and therefore allows the processing of backscattered spectra in a linear, additive manner. These authors concluded that information about the distribution of spacing between reflectors may be seperated from the information about the incident wave itself and investigated. In addition, they noted that two potentially useful parameters for tissue characterization in vivo are the shape of the cepstrum obtained from soft tissue echoes, and attenuation coefficient estimation by the cepstral smoothing of the log power spectra.

Chu and Raeside[6] adopted a frame work for automated pattern recognition applied to M-mode cardiac scans. The steps involved in the analysis consist of processing, feature extraction, and classification. The processing of anterior mitral leaflet waveforms consisted of determining the Fourier series of each waveform obtained from a sample space of 88 subjects (57 normal volunteers and 31 confirmed cases of mitral stenosis). The power spectrum generated by the Fourier series was used to form a 21 component feature vector. Feature ranking was carried out to eliminate less informative components, thus reducing the feature vector to only two componenets. Utilizing this vector Chu and Raeside[6] attempted to establish an effective algorithum for the automated classification of anterior mitral leaflet waveforms of unknown pathology.

Investigated were the nearest-neighbor and Bayes' classifiers. Both classifiers proved extremely successful (not a single miscalculation occurred within the 88 applications).

Preston, Czerwinski, and Leb[7] have investigated sixty-five features based on the shape and statistical properties of the power spectrum, the rectified waveform, and the raw waveform. These features were then processed in order to select the best discriminators between groups of data. Upon application of the discrimination features to the back-scattered signals from normal and pathological (acute pyelonephritis) rabbit kidneys the best results were derived from the frequency spectrum, in particular, from the total energy in the range 0 to 1.8 MHZ and 1.9 to 2.8 MHZ, and from the first moment of the power spectrum.

The above review has been concerned with those techniques using frequency domain analysis. It is, however, important to realize that the frequency domain does not contain any new information about the time domain signal, since it is derived from the latter. Frequency domain analysis is used in this thesis for two reasons: first, the work done by Preston, et al.[7] seems to indicate that frequency domain features tend to be better discriminators; and, second, the attenuation effects of overlying tissue are more readily discerned in the frequency domain.

The following sections of this chapter outline some fundamental physical concepts regarding the interaction of ultrasound with biological tissue.

1.2 WAVE MOTION

In the following sections of this chapter it will be assumed that the energy of an acoustic wave exists at a single frequency unless otherwise stated. Additionally, the medium through which this wave travels is presumed to be isotropic and perfectly elastic. The mode of the wave considered is longitudinal; that is, the particle motion is in the same direction as the energy flow. Additional assumptions will be presented when appropriate to the development.

The mechanisms by which sound energy propagates can be attributed to the elasticity and to the density of the medium. The elasticity, represented by the adiabatic compressibility (κ) of the medium, accounts for the restoring forces that a volume exhibits against compression. The density is represented by the inertia of the mass which results in an overshoot of the particles from their mean position. The resultant particle motion is thus harmonic.

For perfect gasses it can be shown that the group velocity[†] of the wave is proportional to the square root of the mean-squared molecular velocity (Ingard[8]):

$$c \alpha \sqrt{\langle v^2 \rangle}$$

where $\langle v^2 \rangle$ is the mean-squared molecular velocity.

For liquids and solids the velocity of sound is considerably greater than the root-mean-square velocity of a molecule about its equilibrium position. For lonitudinal waves the velocity of sound can be shown to be (Ingard[8]):

[†] Group velocity is the speed at which energy propagates through a medium.

$$c = \sqrt{\frac{K_a}{\rho}} = \sqrt{\frac{1}{\kappa\rho}}$$

where K_a = adiabatic bulk modulus,

ρ = mean density of medium,

κ = adiabatic compressibility.

The velocity of sound is independent of the amplitude and frequency of the wave to the extent that the excess pressure associated with the ultrasound wave is small compared with the equilibrium pressure. This is required to keep the compressibility, κ, from exhibiting an excess pressure dependence.

It has been observed experimentally that the velocity of sound is dependent on the temperature of the transmitting medium. This may be

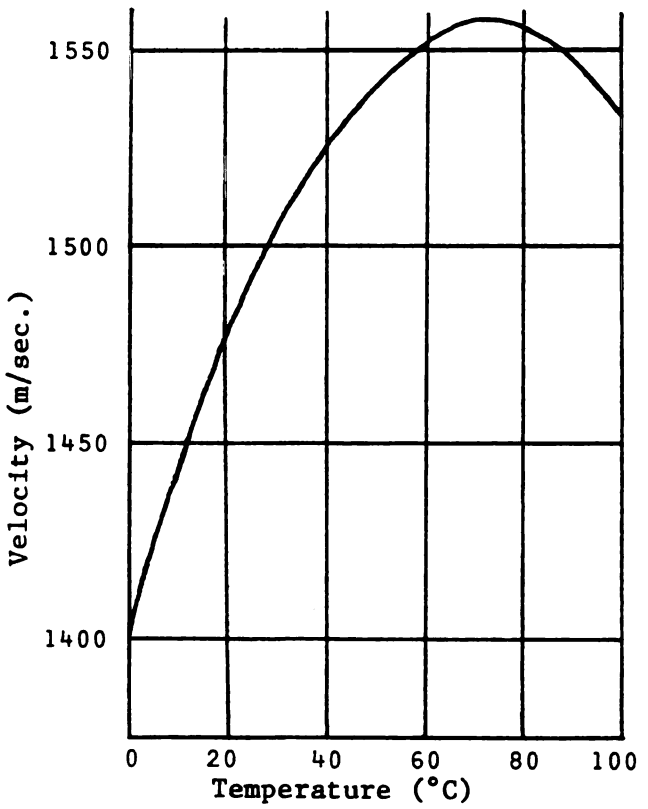

Figure 1.1 Variation of propagation velocity with temperature in water. Wells 1969.

attributed to the temperature dependence of the elasticity and density of the medium. Generally, the relationship between velocity and temperature can be quite complex. Figure 1.1 shows the acoustic velocity versus temperature dependence in distilled water.

Another experimentally observed phenomenon, velocity dispersion, occurs due to the frequency dependence of the acoustic velocity. Velocity dispersion, although measurable, is insignificant for biological tissues in the frequency range of interest ($f < 2.5$ MHZ). The velocity of sound for a few types of biological materials are presented in Table 1.1.

TABLE 1.1

Propagation Velocities of some Biological Materials*

Tissue	Mean Velocity m/sec
Fat	1450
Human tissue, mean value	1540
Brain	1541
Liver	1549
Kidney	1561
Spleen	1566
Blood	1570
Muscle	1585
Skull-bone	4080

* From P.N.T. Wells[9]

1.3 CHARACTERISTIC IMPEDANCE

The characteristic impedance of a medium expresses the relationship between the pressure and phase velocity† associated with propagating acoustic waves. It is defined as:

$$Z = \rho c = \sqrt{\frac{\rho}{\kappa}}$$

where ρ = density,

c = group velocity,

and κ = adiabatic compressibility.

The characterisitic impedance of a medium may be complex (Herzfeld and Litovitz[10] although for biological tissue the imaginary component is negligible (Wells[4]). The relationship between the pressure and phase velocity of the acoustic wave is given by:

$$P = Zu$$

where P = pressure

u = phase velocity,

and Z = characteristic impedance.

The characteristic impedances of a few biological tissues have been tabulated below.

† Phase velocity is the same as the particle vibrational velocity.

TABLE 1.2

Characteristic Impedance of Some Biological Materials*

Tissue	$Z(g/cm^2 \cdot sec) \times 10^{-5}$
Fat	1.38
Brain	1.58
Kidney	1.62
Human tissue, mean value	1.63
Spleen	1.64
Liver	1.65
Muscle	1.70
Skull-bone	7.8

* From P.N.T. Wells[9]

For plane waves incident on a planar interface between two media the characteristic impedances on either side of the interface may be used to define reflection and transmission coefficients. The application of Snell's Law, along with appropriate boundary conditions, lead to an expression for the ratio of the pressure reflected to pressure incident (reflectivity) and the pressure transmitted to the pressure incident (transmissivity). The required boundary conditions are:

1) $$\left.\frac{d\vec{x}}{dt}\right|_{\vec{x} = 0^-} = \left.\frac{d\vec{x}}{dt}\right|_{\vec{x} = 0^+}$$

where $\vec{x}$ = the displacement vector

$\vec{x} = 0^-$ is medium 1 side of boundary

$\vec{x} = 0^+$ is medium 2 side of boundary.

2) $$P(0^-) = P(0^+)$$

where P(x) = pressure of acoustic wave at x.

Thus, the particle velocity and acoustic pressure are continuous at the boundary between two media. The reflectivity and transmissivity are (Ingard[8]):

$$\frac{P_r}{P_i} = \frac{Z_2 \cos\theta_i - Z_1 \cos\theta_t}{Z_2 \cos\theta_i + Z_1 \cos\theta_t}$$

and

$$\frac{P_t}{P_i} = \frac{2 Z_2 \cos\theta_i}{Z_2 \cos\theta_i + Z_1 \cos\theta_t}$$

where Z_1 = characteristic impedance of medium 1

Z_2 = characteristic impedance of medium 2

θ_i = incident angle of acoustic wave from the normal to the planar interface

θ_t = angle of transmitted acoustic wave from the normal to the planar interface.

Snell's law defines the relationship between the angles of incidence and transmission and the acoustic velocity of each medium:

$$\frac{\sin\theta_i}{\sin\theta_t} = \frac{C_1}{C_2}$$

where c_1 = acoustic velocity in medium 1

c_2 = acoustic velocity in medium 2

θ_i = angle of incidence

θ_t = transmitted angle

Figure 1.2 below indicates the angles involved.

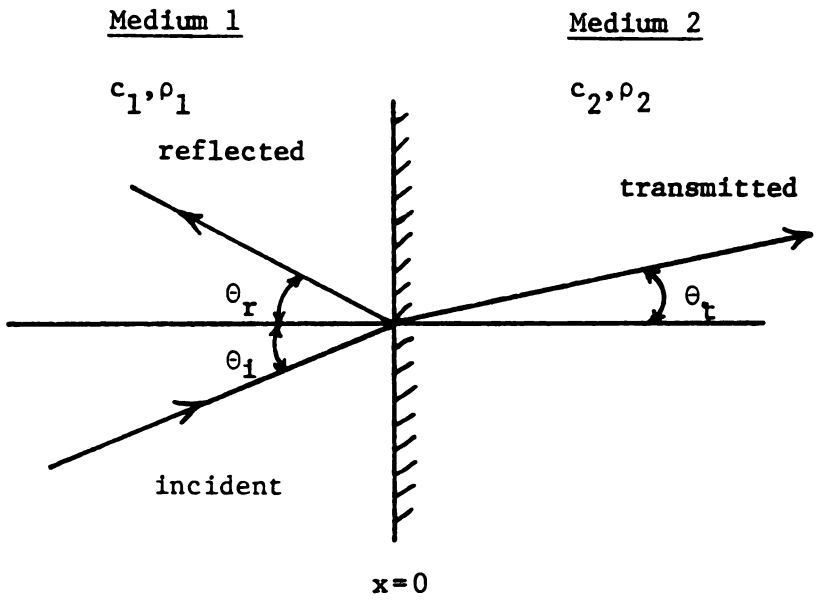

Figure 1.2 Reflection and transmission of acoustic wave.

For the case of normal incidence we have:

$$\theta_i = \theta_t = 0$$

thus

$$\frac{P_r}{P_i} = \frac{Z_2 - Z_1}{Z_2 + Z_1}$$

and

$$\frac{P_t}{P_i} = \frac{2\,Z_2}{Z_2 + Z_1}$$

A similar relationship for the intensity reflection coefficient, (Γ_r), and the intensity transmission coefficient, (T_t), may be developed:

$$\Gamma_r = \left(\frac{Z_2 \cos\theta_i - Z_1 \cos\theta_t}{Z_2 \cos\theta_i + Z_1 \cos\theta_t}\right)^2 = \left(\frac{P_r}{P_i}\right)^2$$

and

$$T_t = \frac{4\, Z_2\, Z_1\, \cos^2\theta_i}{(Z_2\, \cos\theta_i + Z_1\, \cos\theta_t)^2} = \frac{Z_1}{Z_2}\left(\frac{P_t}{P_i}\right)^2$$

Reflections from certain tissue surfaces and large interfaces may be treated approximately in this manner.

1.4 ACOUSTIC SCATTERING

Usually, the scattering processes associated with biological tissue are extremely complex due to the randomness of the size, shape, distribution, orientation, density, and compressibility variations of the scattering centers. As a first step, the solution to the single body scatterer is formulated. Then, utilizing the linearity of the wave equation describing the propagation properties of the medium, the principle of superposition is used to describe multiple body scattering. Unfortunately, even problems of relative simplicity generate rather complex solutions as will be seen in Chapter 2. A more tractable approach to modeling random reflectors in biological tissue is that of Kuc et al.[11] who model the reflectors as a random linear filter. The filter is assumed to have an impulse response that is a zero mean, white Gaussian process. The advantage of this type of approach is that probability and statistics may be applied to the macrostate of the scattering volume, as opposed to a prohibitively complex microstate approach which would attempt to analyze each acoustic wave-reflector interaction separately.

1.5 ATTENUATION

A change in the average cross-sectional acoustic beam intensity may be attributed to either spatial dispersion in the medium through which the wave propagates or to the spatially dependent shape of the acoustic beam characteristic of the transducer itself. This latter phenomenon will be discussed in Section 2.6. Ultrasound attenuation may be due to the combined effects of several different mechanisms, however in certain situations one particular mechanism may predominate. The following section reviews those mechanisms applicable to biological tissue.

A mechanism of attenuation, characteristic of the transmission medium, is the elastic scattering suffered by an acoustic wave as it impinges on discontinuities within the interrogated volume. This leads to a dispersion of the acoustical energy from the original beam direction. Mechanisms of attenuation due to active absorption, however, are related to the visosity, thermal conductivity, relaxation, and elastic hysteresis. Of these mechanisms relaxation is the predominant factor involved in attenuation for biological tissue.

Attenuation due to the transmission of ultrasound through biological tissue is well characterized experimentally by the relation:

$$I = I_o \, e^{-\alpha(f)d}$$

where I_o = initial intensity of acoustic beam,

d = total transmission distance through attenuation medium,

and $\alpha(f)$ = attenuation coefficient characteristic of medium.

In general, the frequency dependence of the attenuation coefficient (α) in biological tissues is linear (Lizzi et al.[4])

$$\alpha \simeq \alpha_o f$$

where

α_o = attenuation per cm at 1 MHZ

and f = frequency of acoustic wave in MHZ.

A table of biological tissues and their corresponding attenuation coefficients are given below. In this table, the absorption coefficient is expressed in terms of dB/cm, rather than inverse centimeters.

TABLE 1.3

Biological Attenuation Coefficients*

Tissue	α/f dB/cm · MHZ	Temp. °C	Frequency MHZ	Com.
Liver, Human	1.17	body	1.5	in vivo
Liver, Human	1.24	40°C	0.97	fresh
Liver, Porcine	1.18	25°C	4	fresh
Liver, Porcine	0.23	24.8°C	4	homogenated
Spleen, Human	0.50	18.2°C	1.6	fixed
Fat, Human	0.6	37°C	1	fresh
Muscle, Human	0.64	37°C	1.5	in vivo
Abdominal Wall	2.94	-	1	fat & muscle
Abdominal Wall	1-2	-	1	mainly fat

* From Comprehensive Compilation of Emperical Ultrasonic Properties of Mammalian Tissue[12]

CHAPTER II

THEORETICAL CONSIDERATIONS

It is instructive to review an approach describing the propagation and scattering of acoustic energy by the appropriate wave equation and boundary conditions. In this chapter the wave equation approach is used to provide a foundation on which to base a linear model. This model provides a useful conceptual tool for analyzing the ultrasound/tissue interaction.

2.1 HOMOGENEOUS MEDIUM

The wave equation approach is often described in terms of a continuous wave field, although ultrasonic excitations generated in practice are of a transient nature. It has been shown, however, that the transient (pulse-echo) and steady state (continuous wave) formulations are equivalent (Goldberg and Watson[15]).

Consider first the wave equation for longitudinal waves in a homogeneous elastic medium for which there is no scattering (Ingard[8]):

$$\nabla^2 p - \frac{1}{c_o^2} \frac{\delta^2 p}{\delta t^2} = 0 \qquad (1)$$

where the pressure, p, is a function of both time and spatial coordinates, and c_o is the group velocity of he acoustic wave. Seperation of the variable $\vec{r}$ (spatial vector) and t (temporal variable) leads to:

$$\nabla^2 p(\vec{r}) + k_{on}^2 \, p(\vec{r}) = 0 \qquad (2)$$

where k_{on} is the wave number, equal to $2\pi/\lambda_n$ and λ_n is the wavelength of the propagating wave. The magnitude of the acoustic wave is assumed to be small so that the velocity and thus wave number are essentially independent of the wave amplitude (i.e. the compressibility and density of the medium do not vary significantly from their mean values). This assumption is valid for intensity levels used in this research and in clinical diagnostic systems. The solution of equation (2) is:

$$p(\vec{r}) = A_n \, e^{j\vec{k}_{on} \cdot \vec{r}} \tag{3}$$

where A_n is the wave amplitude and $\vec{k}_{on}$ is the propagation vector. Introducing the time dependence yields the total solution of the wave equation:

$$P_n(\vec{r},t) = A_n \, e^{j(\vec{k}_{on} \cdot \vec{r} - \omega_n t)} \tag{4}$$

where

$$\omega_n = c_o \, k_{on}$$

By superposition, a more general expression for propagating continuous waves satisfying equation (1) is given by:

$$P(\vec{r},t) = \sum_{n=0}^{\infty} A_n \, e^{j(k_{on} \cdot \vec{r} - \omega_n t)} \tag{5}$$

2.2 WEAKLY INHOMOGENOUS MEDIA

The 'diffuse' echoes observed in a backscattered acoustic wave from biological tissue samples may be attributed to small inhomogeneities within the tissue volume. The wave equation approach becomes complex for such scattering and requires linearization to attain

tractable solutions. An approach of this kind still proves useful in modeling such complex scattering phenomenon.

Consider the case where the compressibility and density of a well defined volume embedded in a homogeneous medium vary as a function of location and thus produce a spatially varying acoustic velocity within the subvolume. The refractive index reflects this variation, as shown in the following expression:

$$n(\vec{r}) = \frac{c_o}{c(\vec{r})} = n_o + n_1(\vec{r}) \tag{6}$$

where c_o is the speed of sound for the homogeneous medium and $c(\vec{r})$ is the speed of sound at a specific location. The n_o term represents the nominal refractive index for the medium, and $n(\vec{r})$ represents small variations about the mean. Starting with equation (2) of the previous section, the Helmholtz equation becomes:

$$\nabla^2 p(\vec{r}) + k^2(\vec{r})p(\vec{r}) = 0 \tag{7}$$

where $k^2(\vec{r})$ may be expressed as:

$$k^2(\vec{r}) = \frac{\omega^2}{c^2(\vec{r})} = \frac{\omega^2}{c_o^2}\frac{c_o^2}{c(\vec{r})} = k_o^2(n(\vec{r}))^2$$

Substituting this into equation (7) yields:

$$\nabla^2 p(\vec{r}) + k_o^2(n_o + n_1(\vec{r}))^2 p(\vec{r}) = 0 \tag{8}$$

One may choose, without loss of generality, $n_o = 1$ (i.e., the nominal acoustic velocity of the inhomogeneous volume is the same as that of the surrounding homogeneous medium). In addition, by the small variation assumption ($n_1 << n_o$) the n_1 terms may be neglected. Equation

(8) becomes:

$$\nabla^2 p(\vec{r}) + k_o^2 p(\vec{r}) \simeq -2\, n_1(\vec{r}) k_o^2 p(\vec{r}) \tag{9}$$

For weak scattering the total pressure field within the inhomogenous volume may be written as the sum of the incident and weakly scattered fields (Gore and Leeman[16]):

$$p_t = p_i + p_s \tag{10}$$

The homogeneous wave equation (2) together with equation (10) results in the following relation:

$$\nabla^2 p_s(\vec{r}) + k_o^2 p_s(\vec{r}) \simeq -2\, n_1(\vec{r}) k_o^2 \{p_i(\vec{r}) + p_s(\vec{r})\} \tag{11}$$

It is possible to formulate the solution for the backscattered acoustic pressure described by (11) at a point, R, using a Green's function. In the far field Waag et al., have shown that the scattered wave may be expressed as:

$$p_s(\vec{r}) \simeq \frac{k_o^2 e^{jk_oR}}{2\pi R} \int_{V'} \{p_i(\vec{r}') + p_s(\vec{r}')\} n_1(\vec{r}') e^{jk_o \vec{r}' \cdot \hat{z}} dV' \tag{12}$$

This expression assumes that the observation point is sufficiently removed from the scattering volume to justify the Fraunhofer condition:

$$\frac{k_o d^2}{2R} << 1 \tag{13}$$

Figure 2.1. depicts the geometry appropriate to equation (12).

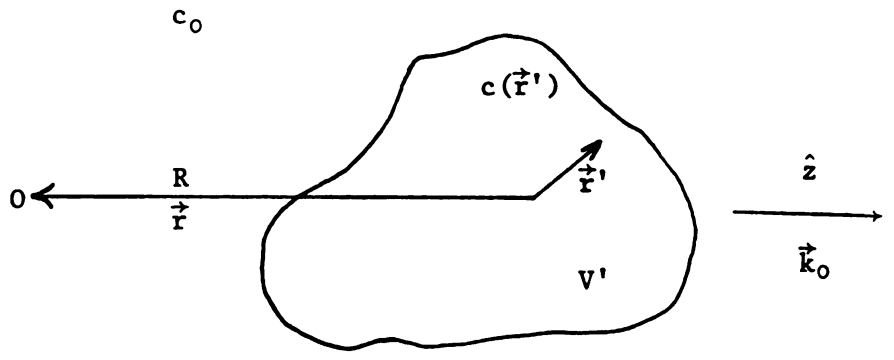

Figure 2.1. Definition of coordinates. Observation point is at location 0. The $\vec{k}$ direction lies in the unit vector, $\hat{z}$, direction.

Equation (11) may be linearized by dropping the scattered pressure term from the integral, consistent with the assumption of weak scattering, thus:

$$p_s(\vec{r}) \simeq \frac{k_o^2 e^{jk_oR}}{2\pi R} \int_{V'} p_i(\vec{r}')n_1(\vec{r}')e^{jk_o\vec{r}'\cdot\hat{z}}\, dV' \qquad (14)$$

Consider a plane wave with amplitude A incident on volume V' such that:

$$p_i(\vec{r}) = Ae^{jk_o\hat{z}\cdot\vec{r}'} \qquad (15)$$

The solution for the backscattered radiation, $p_s(\vec{r})$, is (Wagg[17]):

$$p_s(\vec{r}) \simeq \{Ae^{jk_oR}\}\{\frac{k_o^2}{2\pi R} \int_{V'} n_1(\vec{r}')e^{-jk_o\hat{z}\cdot\vec{r}'} dV'\} \qquad (16)$$

or

$$p_s(\vec{r}) \quad p_i(\vec{r}) \left\{ \frac{k_o^2}{2\pi R} \int_{V'} n_1(\vec{r}') e^{-jk_o \hat{z} \cdot \vec{r}'} \, dV' \right\} \tag{17}$$

The bracketed term in equation (17) represents the reflection coefficient for the scattering volume V'. In general the reflection coefficient is a complex quantity that may be characterized by a magnitude and phase. The important result of equation (17) is the linear relation between the scattered and incident acoustic waves.

2.3 WAVE ATTENUATION

The attenuation of acoustic energy as it propagates through biological tissue has not been considered thus far. Attenuation may be phenomenologically introduced into the above relation by introducing a complex wave number, $k = k_r + jk_i$. The imaginary part of k is often refered to as the attenuation coefficient, α. The introduction of this factor modifies equation (17) as follows:

$$p_s(r) \simeq \{e^{-\alpha R}\} \, p_i(\vec{r}) \left\{ \frac{k_o^2}{2\pi R} \int_{V'} n_1(\vec{r}') e^{-jk_o \hat{z} \cdot \vec{r}'} \, dV' \right\} \tag{18}$$

or

$$p_s(r) \simeq A(f) \, R(f) \, p_i(\vec{r})$$

where

$\alpha = \alpha_o f$ as in section 1.4,

A(f) = the first bracketed term, represents the effect of overlying tissue attenuation, and

R(f) = the second bracketed term, represents the reflection coefficient.

2.4 LINEAR MODELING

The wave equation approach reviewed in the previous sections indicates that an appropriate linear model may be formulated so as to characterize the ultrasound/tissue interaction. This model provides a concise description of the system from which each contributing factor is easily identified.

Figure 2.2 below illustrates the various components involved in the formulation of the linear model. The received signal from a reflector internal to the tissue volume may be written as:

$$y(t) = e(t)*h(t)*b_1(t)*a(t)*r_i(t)*a(t)*b_2(t)*h(t) \quad (20)$$

where all processes are assumed linear, '*' denotes convolution, and

$e(t)$ = transducer excitation waveform,

$h(t)$ = impulse response of piezoelectric transducer,

$b_1(t)$ = transmissivity impulse response for water/tissue interface,

$a(t)$ = impulse response function accounting for attenuation through overlying tissue,

$r_i(k)$ = reflectivity impulse response associated with the r_i scattering volume, and

$b_2(t)$ = transmissivity impulse response for tissue/water interface.

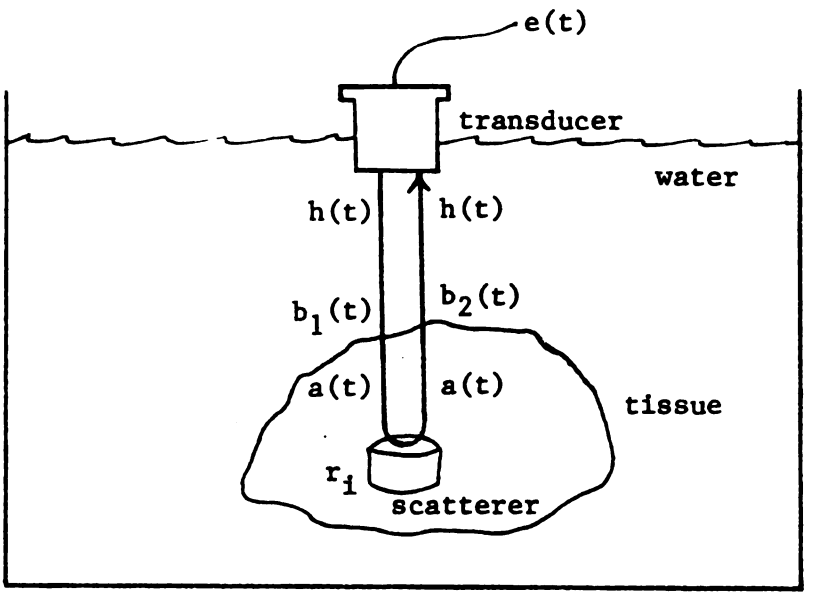

Figure 2.2. Relations involved in linear modeling.

Equation (20) may be written in the frequency domain as:

$$Y(f) = E(f)\ H^2(f)\ A^2(f)\ B_1(f)\ B_2(f)\ R_i(f) \tag{21}$$

Where capitalized letters denote Fourier transforms of their corresponding time domain functions.

Equation (21) shows explicity the dependence of the received signal not only on scattering and attenuation parameters associated with the tissue but also on the form of the interrogating beam. The first two terms may be consolidated to form one term representing the interrogation beam:

$$X(f,d) = E(f)\ H^2(f,d) \tag{22}$$

The distance dependence, d, not as yet considered, has been introduced here and will be discussed in the following section.

The transmissivity coefficients for water/tissue and tissue/water

interfaces are both nearly unity so that equation (21) may be simplified as follows:

$$Y(f,d) \simeq X(f,d)\ A^2(f)\ R_i(f) \tag{23}$$

The transfer or 'tissue signature' function, TS, may be defined as the ratio of the received signal to the interrogating beam signal, or:

$$TS(f,d) = \frac{Y(f,d)}{X(f,d)} = A^2(f)\ R_i(f) \tag{24}$$

Equation (24) indicates that TS(f,d) may be obtained from Y(f,d), if X(f,d) is observable by deconvolution of Y(f,d) and X(f,d). In addition, equation (24) emphasizes the fact that tissue signatures of backscattered ultrasound are due both to the scattering element and the overlying tissue.

2.5 THE STEADY STATE TRANSDUCER FIELD

For practical transducers the acoustic field is rather complex, exhibiting a spatial dependence characterized by two distinct regions, namely; the near (Frésnel) and far (Fraunhofer) zones. A relationship for the central axis intensity distribution may be formulated by assuming that the transducer is a cophasally vibrating piston, and is given by (Wells[9]):

$$I_x = I_o \left\{\sin^2\left(\frac{\pi}{\lambda}\left(\sqrt{r^2 + x^2} - x\right)\right)\right\} \tag{25}$$

where I_o = maximum wave intensity,

I_x = wave intensity at a distance x from the transducer,

r = radius of transducer,

λ = wavelength in propagating medium = c/f,

c = acoustic velocity in medium,

and f = cyclic frequency.

In addition, the beam cross-section intensity exhibits a transverse spatial variation which is dependent upon the distance from the transducer, x, and the ratio r/λ. The number of maxima increase with decreasing values of x and increasing values of r/λ. Figure 2.3 demonstrates both spatial variations for a 1.5 MHz transducer with a radius of 1 cm.

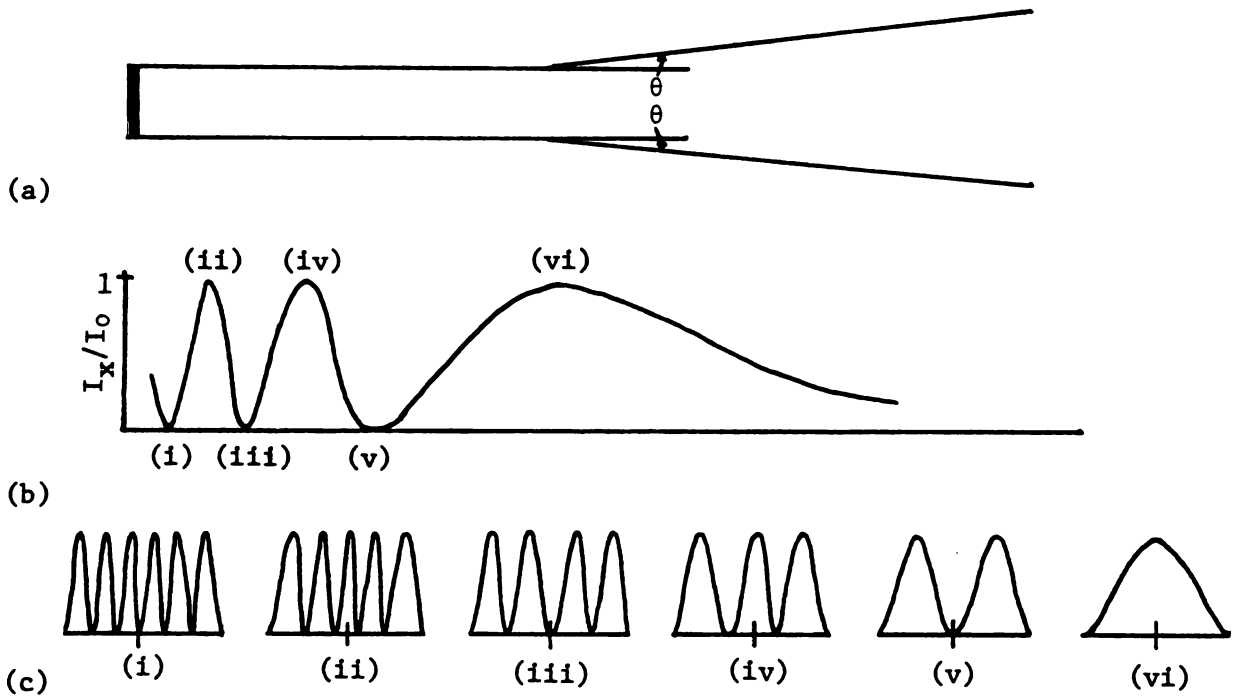

FIGURE 2.3. The ultrasonic field for a 1.5 MHz transducer of radius r=1 cm. (a) most of energy lies within limits shown in this diagram; (b) relative intensity distribution along central axis; (c) relative cross-section intensity distribution for positions indicated in (b).

Axial maxima and minima may be determined using equation (25) and are given by:

$$x_{n,min} = \frac{r^2 - n^2\lambda^2}{2n\lambda}, \tag{26}$$

and

$$x_{m,max} = \frac{4r^2 - \lambda^2(2m+1)}{4\lambda(2m+1)} \tag{27}$$

where

$x_{n,min}$ = position of axial minimum amplitude,

$x_{m,max}$ = position of axial maximum amplitude,

$n = 1,2,3 \ldots$

and $m = 0,1,2 \ldots .$

The directivity function for the far field of the transducer may be defined as (Wells[9]):

$$D_s = \frac{2J_1 (k\, r\sin\theta)}{k\, r\sin\theta} \tag{28}$$

where

J_1 = Bessel's function of the first kind,

and

$k = 2\pi/\lambda$ is the wave number.

At the roots of the Bessel's function the directivity function goes to zero. This indicates that for any angle θ such that $k\, r\sin\theta$ is a root of J_1 the intensity on the surface of a cone defined by the angle θ is zero. The angle of the first null is:

$$\theta \simeq \sin^{-1}\{ \frac{3.83}{kr} \} \tag{29}$$

Figure 2.4 is a polar plot for the far field (for an acoustic velocity of c = 1540 m/sec) of the transducer considered in Figure 2.3.

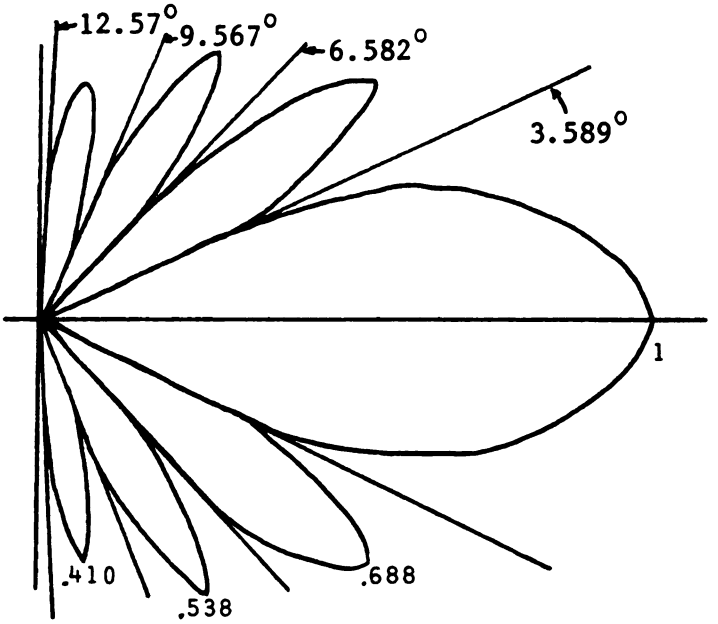

FIGURE 2.4. Polar plot of 1.5 MHz transducer field of radius r = 1 cm. The velocity of sound in the medium is 1540 m/sec.

2.6 IDEAL SCATTERERS

The effects of attenuation due to overlying tissue are investigated for the backscattered power spectrum of three ideal scatterers in this section. To quantify these effects, closed form solutions for eight statistical measures of the spectral power distribution are developed, namely; the mean frequency, variance, skewness, kurtosis, and first through fourth partial sums.

CASE 1: Point Scatterer

For a point scatterer, one whose dimension is much smaller than the acoustic wavelength, the intensity of the secondary scattered wave exhibits an f^4 frequency dependence (i.e. Rayleigh scattering). Attenuation of the acoustic beam due to lossy intervening tissue may be introduced by an attenuation factor, $e^{-2\alpha d}$. The backscattered wave is thus:

$$S_p(f) = R_0 \, f^4 d^{-2\alpha d} \tag{30}$$

where d is the round trip distance traveled by the wave through the attenuating tissue, and R_0 is an arbitrary amplitude factor. Normalization of the above power density function is accomplished by dividing equation (30) by N, defined as:

$$N = \int_{f_\ell}^{f_u} R_0 f^4 e^{-2\alpha d} \, df \tag{31}$$

where

f_u = highest frequency component of interest

and

f_ℓ = lowest frequency component of interest.

Values for the eight statistical measures of the backscattered power spectrum are given by the following expressions (for $\alpha d > 0$ and $f_\ell < f < f_u$):

$$\text{MEAN} = \bar{f}_p = I_{2p}/I_{1p}, \tag{32}$$

$$\text{VARIANCE} = \sigma_{fp}^2 = \{ \, I_{3p} - 2\bar{f} I_{2p} + \bar{f}^2 I_{1p} \, \}/I_{1p}, \tag{33}$$

$$\text{SKEWNESS} = E_p\{(f-\bar{f}_p)^3\} = \{I_{4p} - 3\bar{f}_p I_{3p} + 3\bar{f}_p^2 I_{2p} - \bar{f}_p^3 I_{1p}\}/I_{1p}(\sigma_{fp})^3 \ , \tag{34}$$

$$\text{KURTOSIS} = E_p\{(f-\bar{f}_p)^4\} = \{I_{5p} - 4\bar{f}_p I_{4p} + 6\bar{f}_p^2 I_{3p} - 4\bar{f}_p^3 I_{2p} + \bar{f}_p^4 I_{1p}\}/I_{1p}(\sigma_{fp})^4 \ , \tag{35}$$

$$\text{PARTIAL SUMS} = PS_{np} = I_{1p}\Big|_{f_n}^{f_{n+1}} \Big/ I_{1p}\Big|_{f_\ell}^{f_u} \quad (n = 1,2,3,4) \ , \tag{36}$$

where

$$f_n = (f_u - f_\ell)(n-1)/4 + f_\ell \ , \tag{37}$$

$$I_{1p} = \int_{f_\ell}^{f_u} f^4 e^{-2\alpha_o df}\, df \ , \tag{38}$$

and

$$I_{mp} = \frac{f^{m+3}}{2\alpha_o d} e^{-2\alpha_o df}\Big|_{f_u}^{f_\ell} + \frac{(m+3)}{2\alpha_o d} I_{(m-1)p} \quad (m = 2,3,4,5) \ . \tag{39}$$

CASE 2: Cylindrical Scatterer

For a long thin cylinder with a diameter much smaller than the acoustic wavelength, the scattered power spectrum is proportional to f^3. Following a similar development as that for the point scatterer, the normalized backscattered power spectrum may be expressed as:

$$S_{Nc}(f) = \frac{R_o f^3 e^{-2\alpha_o df}}{\int_{f_\ell}^{f_u} R_o f^3 e^{-2\alpha_o df}\, df} \quad . \tag{40}$$

The eight statistical measures for the cylindrical scatterer possess the same general form as equations (32) through (38) for the point scatterer, with the exception that the I_{mp}'s are replaced with the following expressions:

$$I_{1c} = \int_{f_\ell}^{f_u} f^3 e^{-2\alpha_o df}\, df \quad , \tag{41}$$

and

$$I_{mc} = \frac{f^{m+2}}{2\alpha_o d} e^{-2\alpha_o df}\Big|_{f_u}^{f_\ell} + \frac{(m+2)}{2\alpha_o d} I_{(m-1)c} \tag{42}$$

$$(m = 2,3,4,5).$$

CASE 3: Planar Scatterer

Specular reflection from a plane with dimensions much larger than the acoustic wavelength is frequency independent. The normalized backscattered spectrum together with attentuation due to overlying tissue may be written as:

$$S_{Npl}(f) = \frac{R_o e^{-2\alpha_o df}}{\int_{f_\ell}^{f_u} R_o e^{-2\alpha_o df}\, df} \tag{43}$$

As with the cylinderical scatterer, the statistical measures characterizing the backscattered power spectrum have the same general form as the point scatterer, with the I_{mp}'s replaced by:

$$I_{1pl} = \int_{f_\ell}^{f_u} e^{-2\alpha_o df}\, df \tag{44}$$

and

$$I_{mpl} = \frac{f^{m-1}}{2\alpha_o d} e^{-2\alpha_o df}\Big|_{f_u}^{f_\ell} + \frac{(m-1)}{2\alpha_o d} I_{(m-1)pl} \tag{45}$$

$$(m = 2,3,4,5) .$$

The above relations for the point, cylinder, and plane scatterers have been applied to the following situations,

1) no overlying tissue {i.e. $\alpha d = 0$},

2) 3 cm of overlying tissue with an attenuation of 0.9 dB/cm - MHz (i.e. $\alpha d = 1.38f$ where f is in MHz),

3) 3 cm of overlying tissue with an attenuation of 1.0 dB/cm - MHz (i.e. $\alpha d = 1.38f$ where f is in MHz).

Two different frequency ranges have been considered, viz., the range from .4 to 1.6 MHz, and the range from 2.9 to 4.1 MHz. The results have been tabulated for the point scatterer in Table 2.1, for the cylindrical scatterer in Table 2.2, and for the plane scatterer in Table 2.3.

TABLE 2.1

POINT SCATTERER

Measure	0.4 - 1.6 MHz Range			2.9 - 4.1 MHz Range		
	Attenuation in dB/cm - MHz			Attenuation in dB/cm - MHz		
	0	.9	1.0	0	.9	1.0
Mean	1.334	1.168	1.144	3.632	3.349	3.320
Variance	0.050	0.084	0.088	0.108	0.105	0.099
Skewness	-1.142	-0.496	-0.414	-0.463	0.536	-.645
Kurtosis	3.979	2.608	2.254	2.116	2.213	2.386
First Partial Sum	0.015	0.079	0.092	0.137	0.407	0.441
Second Partial Sum	0.079	0.205	0.223	0.119	0.282	0.281
Third Partial Sum	0.259	0.325	0.325	0.280	0.189	0.173
Fourth Partial Sum	0.647	0.391	0.360	0.384	0.123	0.104

TABLE 2.2

CYLINDRICAL SCATTERER

Measure	0.4 - 1.6 MHz Range Attenuation in dB/cm - MHz			2.9 - 4.1 MHz Range Attenuation in dB/cm - MHz		
	0	.9	1.0	0	.9	1.0
Mean	1.280	1.076	1.048	3.601	3.319	3.292
Variance	0.065	0.099	0.100	0.113	0.100	0.094
Skewness	-1.021	-0.237	-0.119	-0.350	0.645	0.768
Kurtosis	3.908	2.391	1.989	1.983	2.467	2.506
PS1	0.033	0.148	0.170	0.161	0.444	0.479
PS2	0.116	0.258	0.273	0.213	0.280	0.277
PS3	0.284	0.304	0.296	0.276	0.172	0.157
PS4	0.566	0.291	0.261	0.350	0.104	0.087

TABLE 2.3

PLANE SCATTERER

Measure	0.4 - 1.6 MHz Range Attenuation in dB/cm - MHz			2.9 - 4.1 MHz Range Attenuation in dB/cm - MHz		
	0	.9	1.0	0	.9	1.0
Mean	1.000	0.739	0.717	3.500	3.239	3.217
Variance	0.120	0.081	0.075	0.081	0.081	0.075
Skewness	0.000	0.986	1.085	0.000	0.986	1.085
Kurtosis	1.800	3.199	3.508	1.800	3.199	3.508
PS1	0.250	0.552	0.584	0.250	0.552	0.584
PS2	0.250	0.263	0.255	0.250	0.263	0.255
PS3	0.250	0.215	0.112	0.250	0.125	0.112
PS4	0.250	0.059	0.049	0.250	0.059	0.049

In general, the ability of features to differentiate between scatterer types is dependent upon their sensitivity to scattering properties and relative insensitivity to overlying tissue effects. This has been investigated for the ideal scatterers considered above, and the results tabulated below. From these tables it is observed that there are no features that exhibit the most favorable conditions for both attributes simultaneously. There is a trade off between sensitivity to scatter type and insensitivity to overlying tissue effects. For example the skewness of the power spectrum exhibits high sensitivity to both scatterer type and changes in overlying tissue attenuation (see Tables 2.4 and 2.5). Conversely, the mean frequency is relatively insensitive to both factors. However, it should be noted that, for these ideal reflectors, the sensitivity of each feature to scatterer type is, for the mostpart, greater than that for a 100% change in overlying tissue attenuation.

The backscattered power spectra from biological tissue will be much more complex than those considered here.

TABLE 2.4

RANK ORDER OF MEASURES*

from least to most sensitive to 10% change in overlying tissue attenuation coefficient

	0.4 - 1.6 MHz Frequency Range			2.9 - 4.1 MHz Frequency Range		
	Point Source	Cylinder Source	Plane Source	Point Source	Cylinder Source	Plane Source
Rank						
1	PS3 (<0.31%)	σ^2 (0.10%)	M (2.98%)	PS2 (0.36%)	M (0.81%)	M (0.68%)
2	M (2.05%)	M (2.60%)	PS2 (3.04%)	M (0.87%)	PS2 (1.07%)	PS2 (3.04%)
3	σ^2 (4.55%)	PS3 (2.63%)	PS1 (5.48%)	σ^2 (5.71%)	K (1.56%)	PS1 (5.48%)
4	PS4 (7.93%)	PS2 (5.49%)	σ^2 (7.41%)	K (7.25%)	σ^2 (6.00%)	σ^2 (7.41%)
5	PS2 (8.07%)	PS4 (10.31%)	K (8.81%)	PS1 (7.71%)	PS1 (7.31%)	K (8.81%)
6	PS1 (14.13%)	PS1 (12.94%)	S (9.12%)	PS3 (8.47%)	PS3 (8.72%)	S (9.12%)
7	S (16.53%)	K (16.81%)	PS3 (10.40%)	PS4 (15.45%)	S (15.02%)	PS3 (10.40%)
8	K (17.12%)	S (49.79%)	PS4 (16.94%)	S (15.90%)	PS4 (16.35%)	PS4 (16.95%)

* Where percentages refer to percent change in measure attributed to a 10% change in the attenuation coefficient. Results on this table are generated from columns two and three of Tables 2.1 through 2.3

TABLE 2.5

RANK ORDER OF MEASURES*

from least to most sensitive to scatter type

	0.4 - 1.6 MHz Frequency Range		2.9 - 4.1 MHz Frequency Range	
Rank	Point/ Cylinder	Point/ Plane	Point/ Cylinder	Point/ Plane
1	K (1.82%)	PS3 (3.47%)	M (0.85%)	M (3.63%)
2	M (4.05%)	M (25.04%)	PS3 (1.43%)	PS3 (10.71%)
3	PS3 (8.80%)	K (54.76%)	α^2 (4.42%)	σ^2 (11.11%)
4	S (10.60%)	σ^2 (58.33%)	K (6.29%)	K (14.93%)
5	PS4 (12.52%)	PS4 (61.36%)	PS2 (6.57%)	PS2 (20.40%)
6	σ^2 (23.08%)	PS2 (68.00%)	PS4 (9.71%)	PS4 (34.90%)
7	PS2 (31.90%)	PS1 (94.00%)	PS1 (14.91%)	PS1 (45.20%)
8	PS1 (54.55%)	S (100.00%)	S (24.41%)	S (100.00%)

*Where percentages refer to the percent change in the measures between source types. Attenuation due to overlying tissue is assumed to be 0dB/cm MHz. Results on this table are generated from column one of Tables 2.1 through 2.3.

CHAPTER III

EXPERIMENTAL PROCEDURE AND RESULTS

The spectral energy distribution of backscattered ultrasound ratiation depends not only on the intrinsic properties of the tissue (e.g. ε and κ) but also on the interrogating pulse shape[16]. Therefore, it is necessary to investigate the characteristics of the ultrasonic beam as a function of frequency and distance. For this purpose, analysis of backscattered radiation from a thick metal block, assumed to be a perfect reflector, was performed. The results are presented in Section 3.2.

The remainder of this chapter contains material covering data collection procedures, and tissue differentiation techniques. Section 3.1 outlines the general data collection procedure and post processing of information. Section 3.3 discusses the Mahalanobis distance as applied to tissue differentiation.

3.1 EXPERIMENTAL PROCEDURE

Figure 3.1 depicts the general data collection and signal processing system used for tissue analysis in this thesis. Details of the system operation and performance are contained in previous works[13,14] and also in the appendix. A brief outline is presented below.

Data collection is completely synchronized by the Varian 74 minicomputer. The user has the ability, via the Varian 74, to obtain 160 seperate 'looks' per data file of either A-mode or B-mode scans. Each 'look' corresponds to an echo train generated by a single excitation

of the piezoelectric transducer (see Figure 3.3A). The time varying voltage signal, which is proportional to the backscattered radiation is band limited (low passed at 1.8 MHz with a flat passband and sharp cutoff filter, ≈40 dB. octave and highpassed at 100 KHz) and amplified (selectable gain from 0 to 62 dBO. Analog/Digital Conversion (A/D) is accomplished at 5 MHz, with each sample quantized into one of 256 levels (i.e. 8 bit samples). Each record, containing 2048 samples/waveform, is then stored on magnetic tape for further signal processing.

Software developed for the analysis of backscattered waveforms is discussed extensively in Appendix A. The following is a list of the software features:

A.1) a subroutine to plot the raw data of the backscattered radiation,

A.2) time weighting functions to suppress frequency domain sidelobes,

A.3) the ability to calculate either the amplitude or power spectrum of the weighted time signal via an FFT algorithm,

A.4) subroutines to plot the frequency domain response,

A.5) the ability to calculate ratios between frequency domain distributions (i.e., deconvolution),

A.6) user defined attenuation correction factor that is applied to the frequency domain (i.e., exp (αd)),

A.7) a subroutine to calculate eight statistical measures of the spectral distribution, namely; the mean, variance, skewness, kurtosis, and first through fourth partial sums.

In addition, software has been developed to analyze groups of statistics that have been generated by the spectral analysis of backscattered waveforms originating from the same class of scatterers (e.g. liver, spleen, metal block). The following is a list of features for this software:

B.1) subroutine to calculate the mean and variance for each group of statistics (see A.7 of previous list),

B.2) subroutine to determine the covariance matrix for any feature vector† of the class,

B.3) algorithm for determining the Mahalanobis distance between a sample point and any given test set.

The Mahalanobis distance is defined mathematically as:

$$d^2 = \{\mu_1 - \mu_2\}^T \Sigma^{-1} \{\mu_1 - \mu_2\}$$

where μ_1 = coordinate vector of the centroid of a test set in the given feature space,

μ_2 = coordinate vector of the sample point in the same feature space,

and Σ^{-1} = the inverse covariance matrix of the test set.

Heuristically, the Mahalanobis distance assigns the number, d, to a sample whose relative magnitude may be interpreted as a measure of how similar that sample point is to a given test set. The Mahalanobis distance is discussed further in Section 3.3.

†The feature vector is any subset of the eight statistical measures characterizing the spectra of a class (see A.7 of previous list).

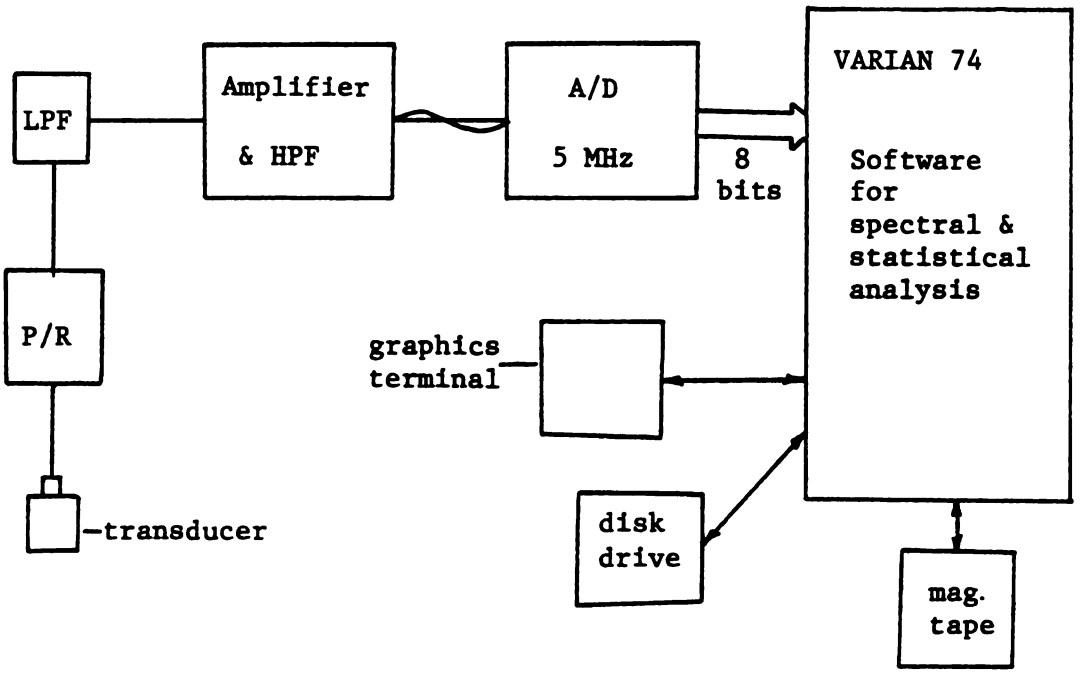

FIGURE 3.1 Data Collection System and Post Processing.

3.2 BACKSCATTER FROM A METAL BLOCK

The radiation field of a practical transducer exhibits a spatial dependence. This has been investigated for the transducer used in this thesis by analyzing the backscattered radiation from a thick metal block. The block was positioned at various distances in the near field of the transducer.

The experimental procedure is outlined below (see Figure 3.2).

1) A metal block (4 cm x 15 cm x 15 cm) was placed at the bottom of a large tank (56 cm x 54 cm x 61 cm) partially filled with distilled water at 27° C.

2) The transducer, supported by a laboratory chemical stand, was positioned at various distances from the metal block. The distances varied from 2 cm to 5 cm in 3 mm increments.

3) With the pulser-receiver continuously pulsing the transducer (≃ once every 1.2 msec) the output of the amplifier

was monitored with an oscilloscope. The amplifier gain was set at 29 dB. The transducer's angular position was varied while the distance from the metal block was held constant so as to produce maximum peaks in the backscattered waveform, indicating normal incidence to the metal block.

4) After achieving proper transducer positioning the pulser-receiver was set to external trigger mode, and data collection was executed via the Varian 74. Two files per transducer position, each containing 95 seperate waveforms, were recorded on magnetic tape.

It should be noted that the transducer is not capable of unabiguously detecting spatial variations of the acoustic wave that are equal to or less than the transducer face dimensions. Therefore, although the near field produces a complicated interference pattern, the waveform produced by the transducer is theintegrated result of all localized field components incident on the entire transducer face. Thus localized nulls or peaks can not be detected.

A typical backscattered time domain waveform from the metal block is presented in Figures 3.3A and B. The transmitted signal occurs at t=0 seconds and the first reflection from the front face of the metal block occurs approximately 52 microseconds later. Additional pulses are due to multiple reflections from both the front and backside of the metal block (see Figure 3.2).

The definition of terms presented here pertain to the remaining discussion on spectral variations of the backscattered radiation from a metal block.

Intradistance spectral class - the set of all spectra determined from the metal block held fixed in orientation and distance with respect to the transducer.

Interdistance spectral class - the set of all spectra determined from one and only one backscattered waveform originating from the metal block placed at each 3 mm increment between 2 cm and 5 cm inclusive with the same orientation (i.e., normal incidence).

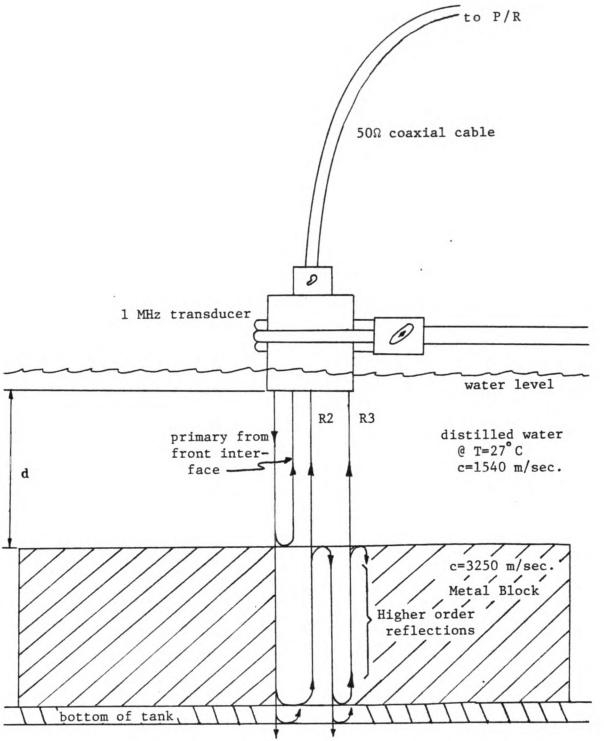

Figure 3.2. Experimental set up for investigation of the ultrasonic field spatial dependence.

Intradistance measure matrix - the N x 8 matrix whose $i\text{-}j^{th}$ element is the j^{th} statistical measure (see A.7 of Section 3.1) of the i^{th} spectrum belonging to an intradistance spectral class. N is the number of different spectra in each class (N=190=2 files each containing 95 records per distance).

Variations in the spectra of backscattered ultrasound from a metal block at constant orientation and distance due to random noise have been investigated. In Figure 3.4 the spectra of six different signal records have been superimposed. Each record was taken at the same position. The results shown in this figure are typical of intradistance spectral classes. Note that most of the variation occurs at the lower frequencies, viz., 0.4 to 0.6 MHz.

The superimposed spectra of two signal records taken at different distances are presented in Figure 3.5. This figure indicates that for reflectors in the near field of the transducer the spectral variations of records belonging to intradistance classes are of the same magnitude as those for interdistance classes.

Interdistance spectral variations of the backscattered radiation in the near field of the transducer have been investigated further. Eight statistical measures (see A.7 of Section 3.1) have been calculated for each member of the intradistance spectral classes. The mean and variance for each column of the intradistance measure matrix have been calculated and plotted versus distance in Figures 3.6 through 3.9. The vertical scaling of each figure is identical to facilitate the comparison of magnitude variations between intradistance mean values of the statistics. Spatial variations of the mean value for the intradistance mean, variance, first partial sum, and fourth partial sum are significantly less than those for the intradistance skewness and kurtosis, and to a lesser

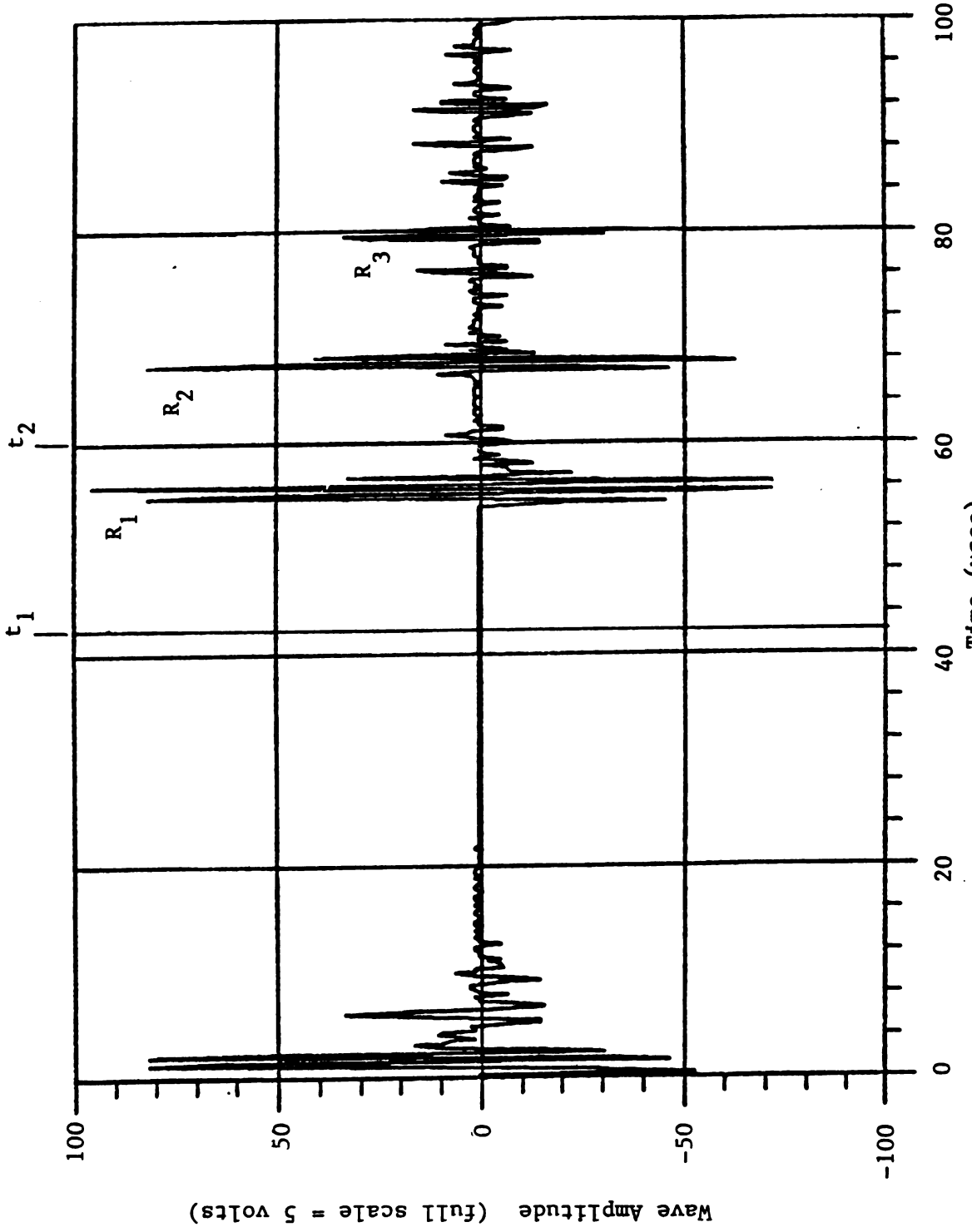

Figure 3.3A Typical sampled backscattered waveform from metal block.
The time window between t_1 and t_2 corresponds to the primary reflection.

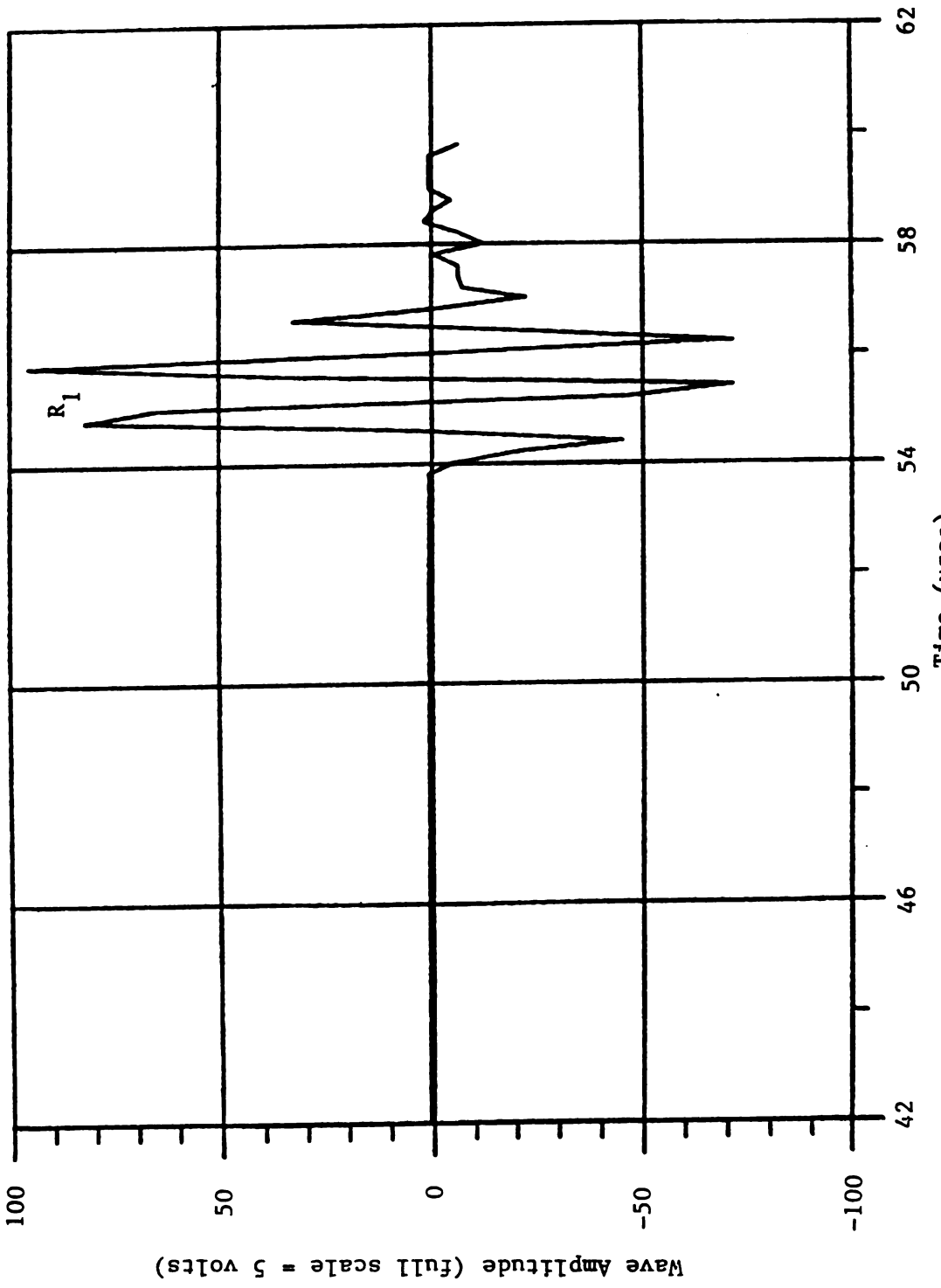

Figure 3.3B Expanded view of Figure 3.3A between t_1 and t_2.

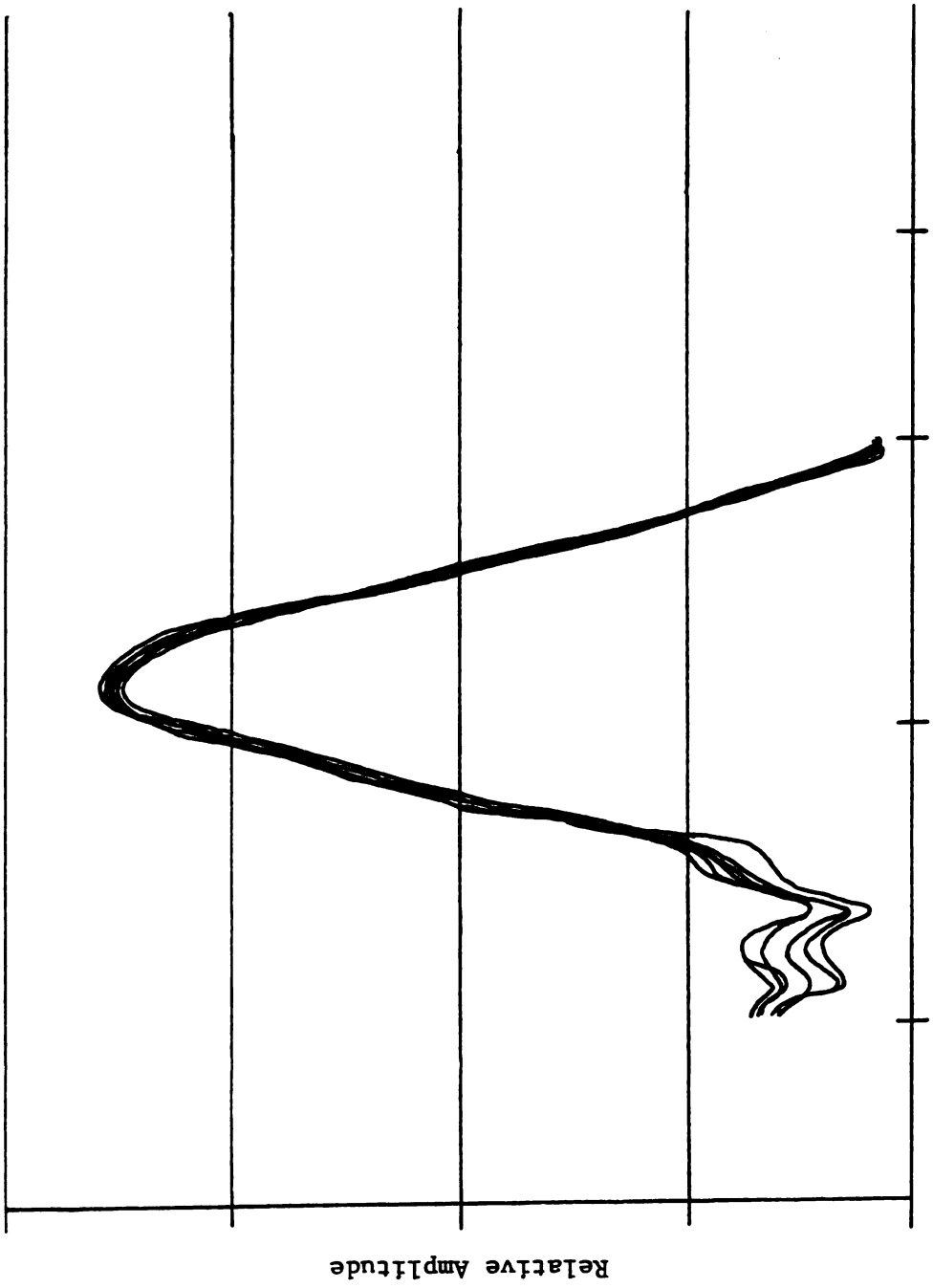

FIGURE 3.4. Frequency spectra for reflection from a metal block at same position but different records.

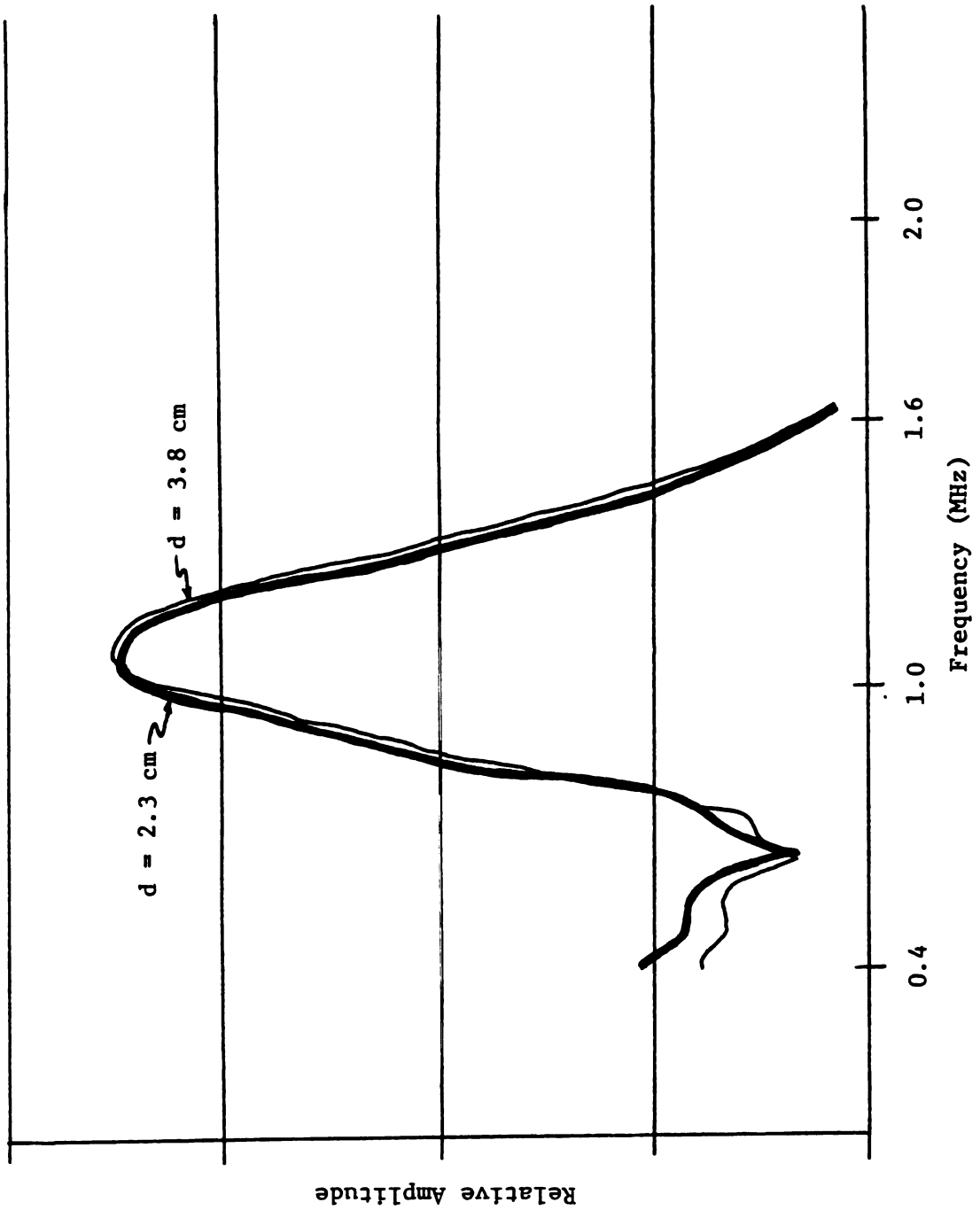

FIGURE 3.5. Frequency spectra of reflections from a metal block for distances d = 2.3 cm and d = 3.8 cm.

extent for the second and third partial sums. This would indicate that the former measures would also exhibit greater stability for reflections from a more complex scatterer that was randomly placed within the near field of the transducer. The ill behaved nature of the intradistance skewness, kurtosis, second and third partial sums presents a problem when the order of magnitude between variations due to reflector type (e.g. liver and spleen) is the same as that for interdistance variations.

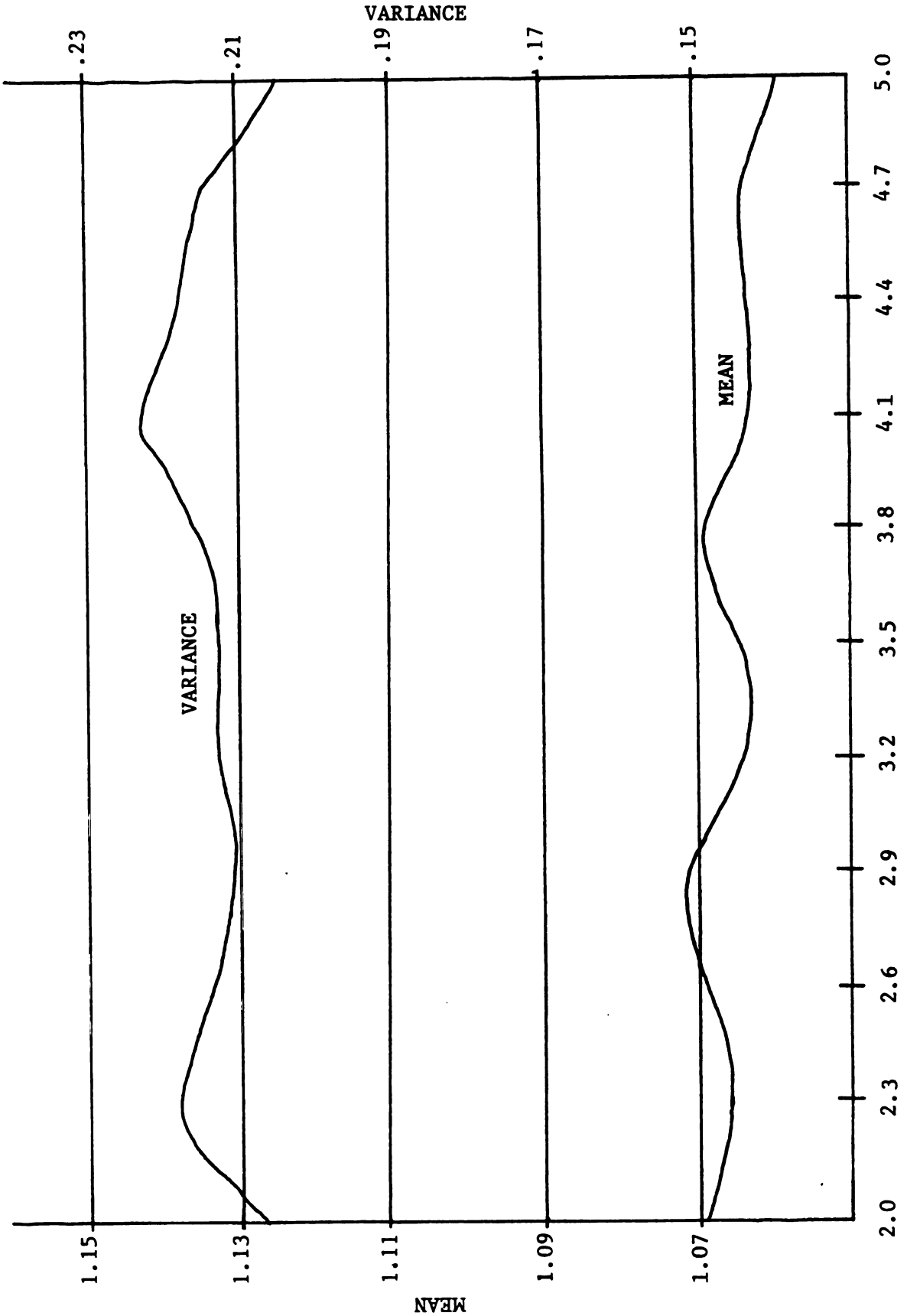

FIGURE 3.6. Intradistance spatial variations of mean and variance.

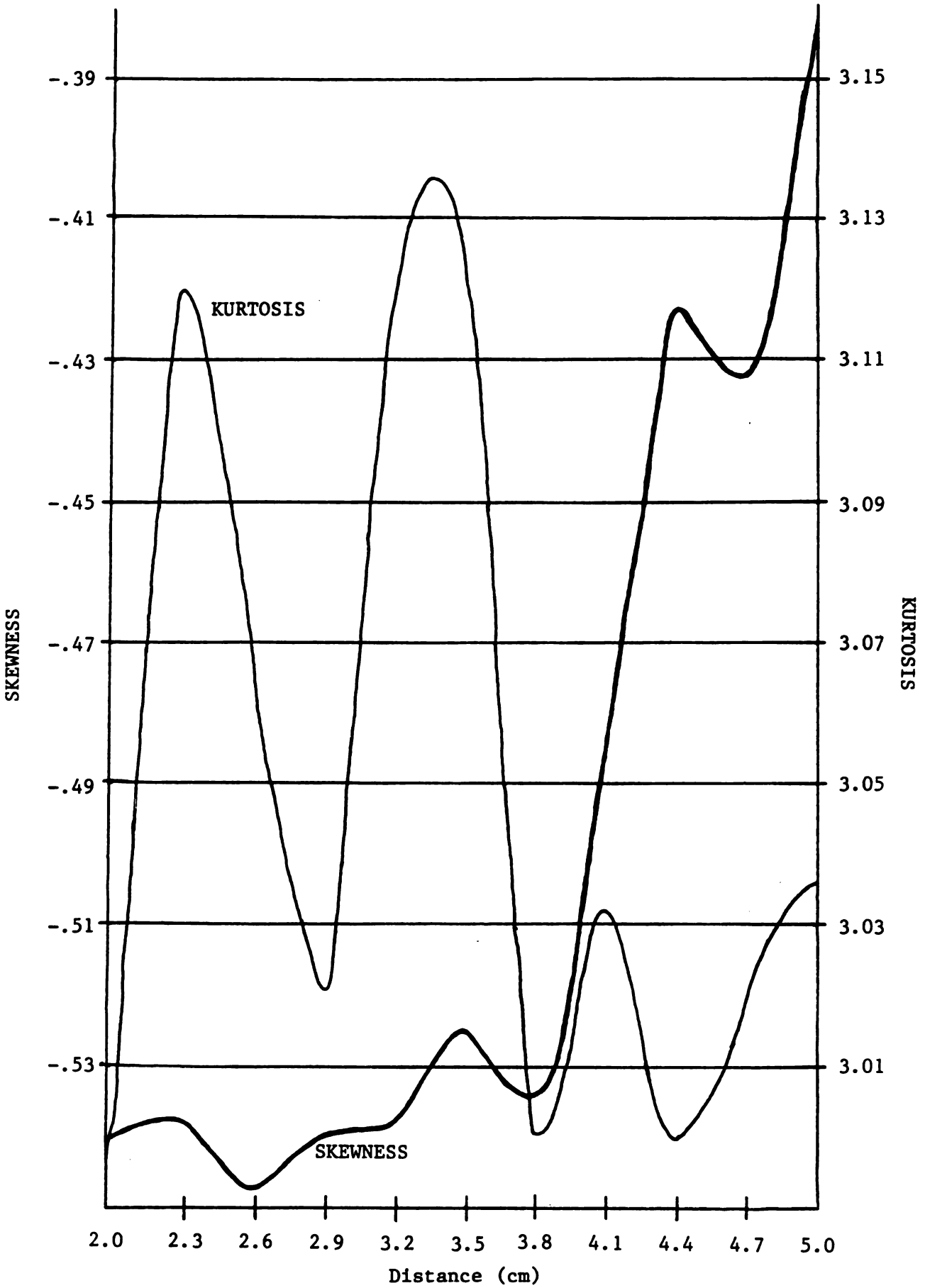

FIGURE 3.7 Intradistance spatial variations of skewness and kurtosis.

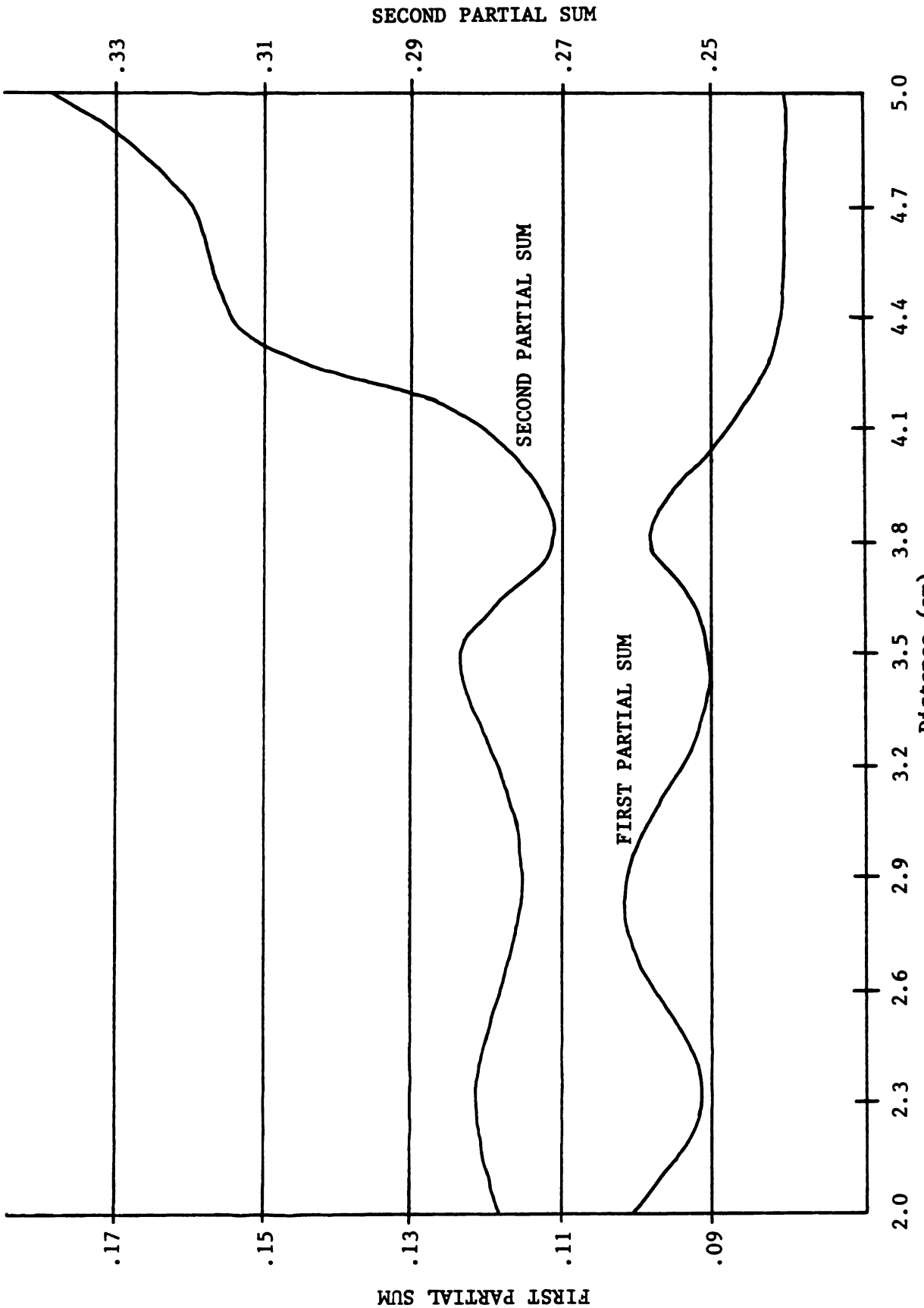

FIGURE 3.8. Intradistance spatial variations of first and second patial sums.

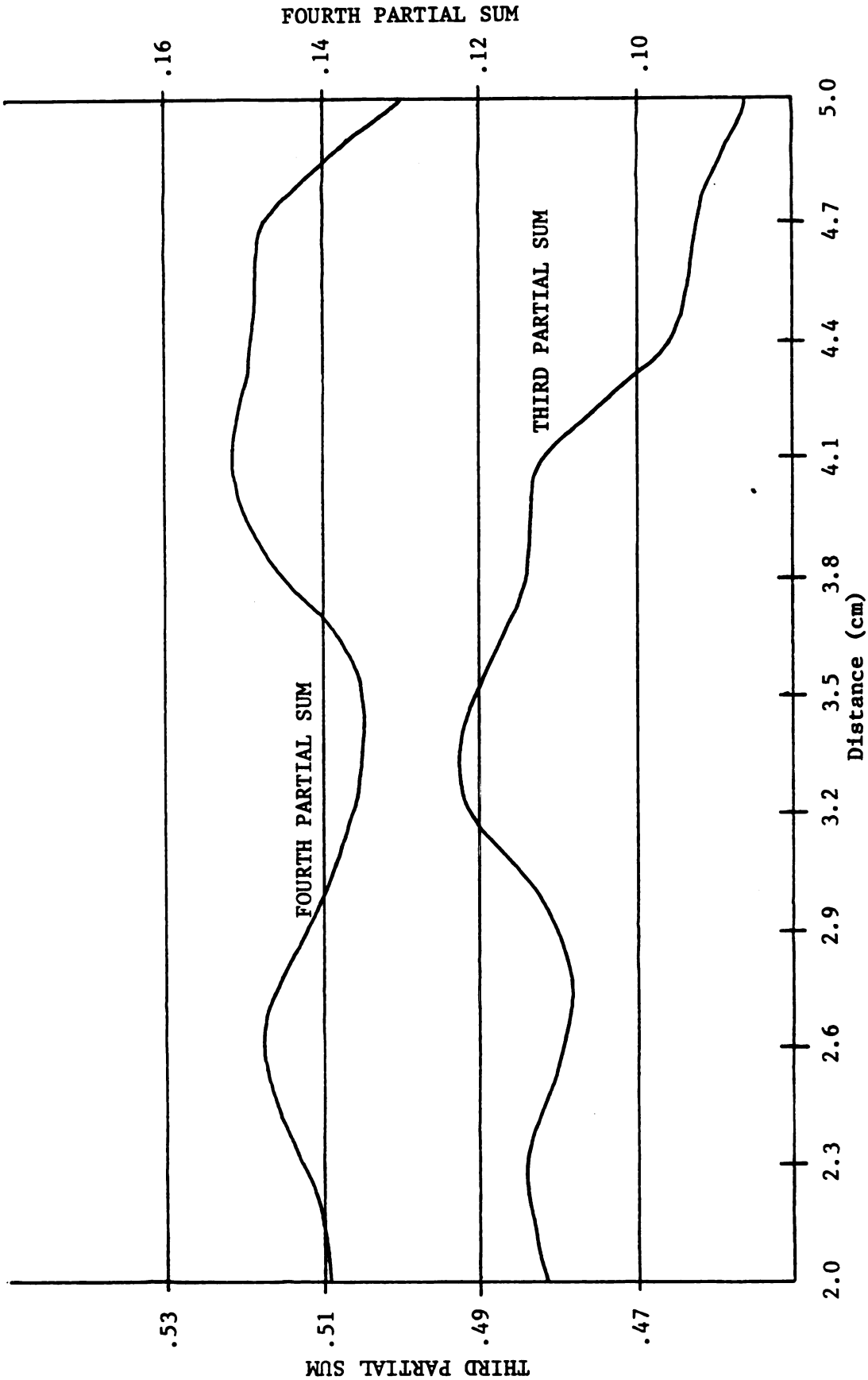

FIGURE 3.9. Intradistance spatial variations of third and fourth partial sums.

3.3 THE MAHALANOBIS DISTANCE

This section reviews the concept of the Mahalanobis distance as it applies to tissue differention. Two illustrative examples consisting of well ordered classes will be presented.

Consider two arbitrary classes whose densities in a two dimensional feature space are contained within the closed contours of Figure 3.10. This figure is not typical of density plots obtained from the analysis of echoes orginating from biological tissue for the features considered in this thesis. It is only presented here as an example.

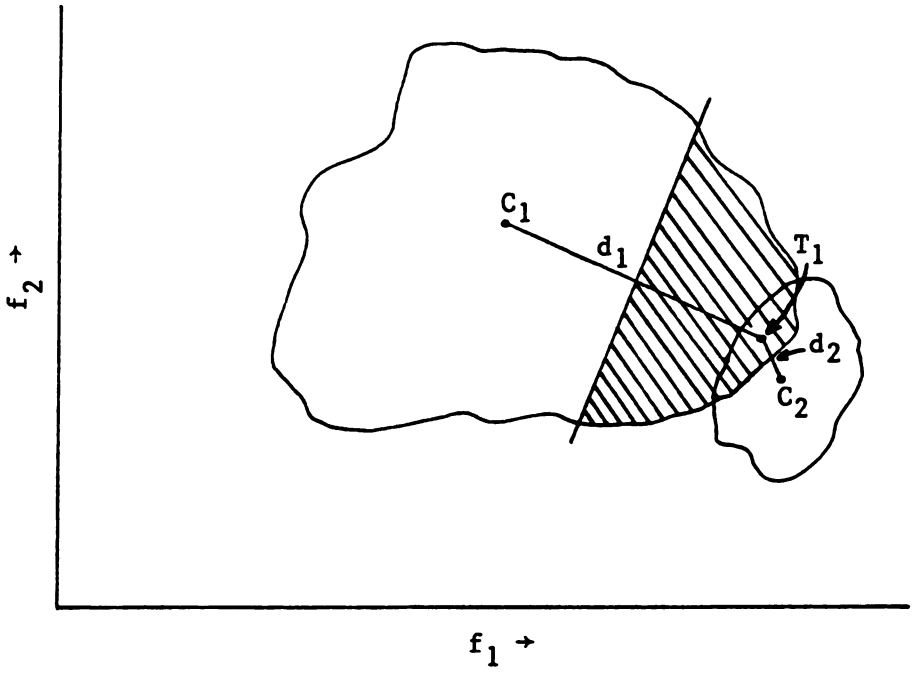

FIGURE 3.10 Bivariate density plot of two arbitrary classes in the feature space (f_1, f_2). The area within the closed contours indicates regions of nonzero density for both classes.

Consider the sample point, T_1, in the above figure. Let the measures d_1 and d_2 be the Euclidean distances from T_1 to the centroids of classes C_1 and C_2 respectively. One method for classigying T_1 would be to assign it to the closest class (i.e., to C_1 if $d_1 < d_2$, and to C_2 if $d_2 < d_1$). The sample point T_1 would be classified as a member of C_2 by this method, which is incorrect. In fact, any point lying in the shaded region of C_1 would be incorrectly classified.

Another method for classifying sample points in a feature space would be to use the same criterion as above with the Mahalanobis distance substituted for the Euclidean distance. The advantage of the Mahalanobis distance is that it takes into account the spread of the classes about their centroids (see equation 3.1). Consider the well ordered classes of Figure 3.11.

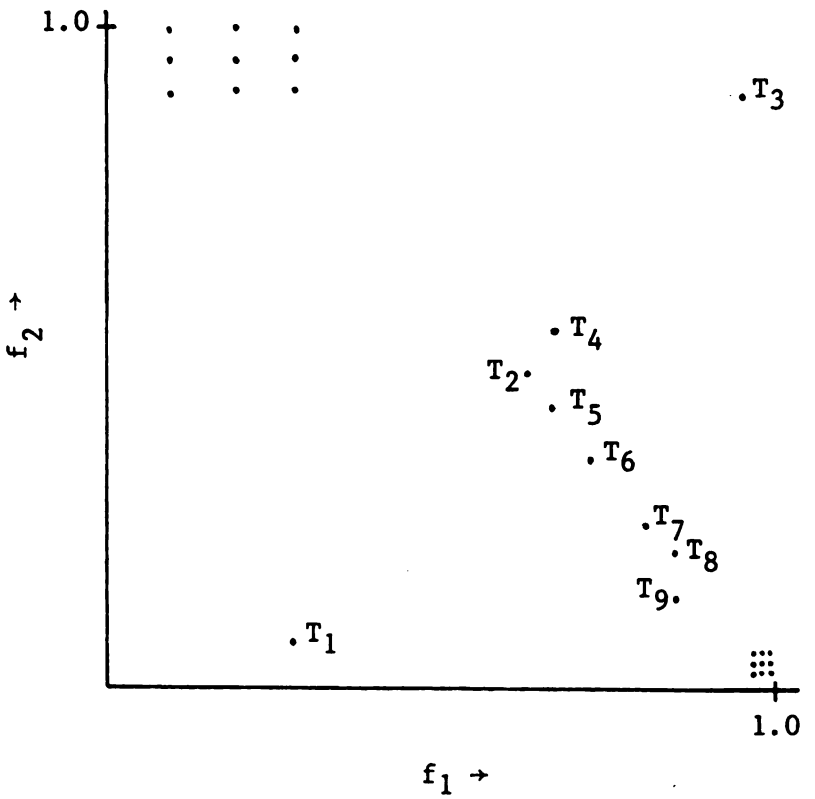

FIGURE 3.11. Example of two well ordered classes in feature space (f_1, f_2).

The Mahalanobis distances for all T_1's have been calculated and are tabulated below.

TABLE 3.1

MAHALANOBIS DISTANCES AND CLASSIFICATION

for all sample points of Figure 3.11

Sample Point	Mahalanobis Distance		
	to C_1	to C_2	Classification
T_1	10.893	11.096	C_1
T_2	10.484	11.088	C_1
T_3	10.030	11.101	C_1
T_4	10.328	11.090	C_1
T_5	10.650	11.075	C_1
T_6	10.758	10.883	C_1
T_7	10.861	10.883	C_1
T_8	10.842	10.925	C_1
T_9	10.878	10.728	C_2

Even for classes that overlap, the Mahalanobis method performs better than does the euclidean as demonstrated by the sketches of Figure 3.12.

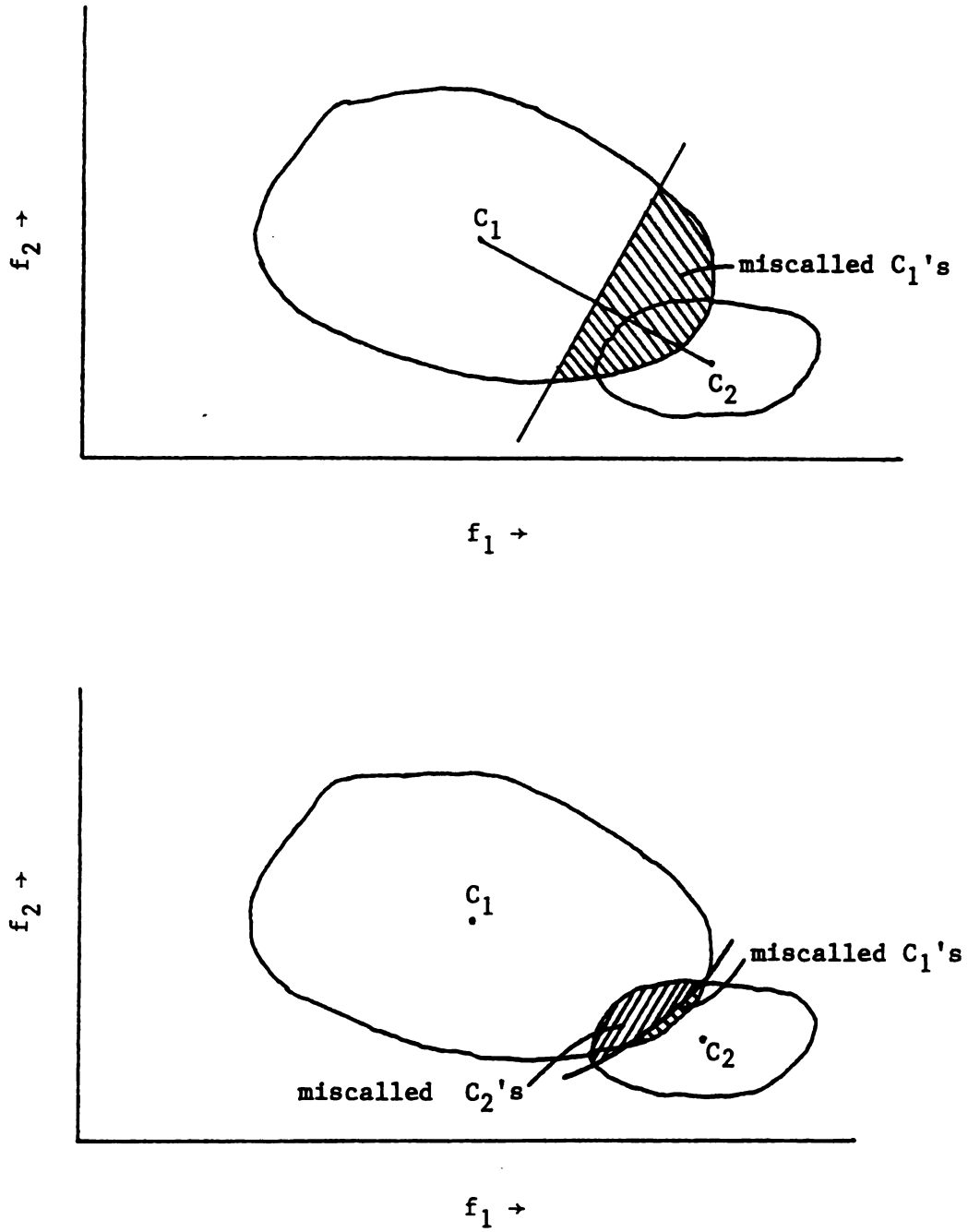

Figure 3.12 a) Classification using the euclidean distance method. Shaded region indicates area where miscalls would occur.

b) Classification using the Mahalanobis distance method. Shaded region indicates areas where miscalls would occur.

CHAPTER IV

BIOLOGICAL TISSUE ANALYSIS

The analysis of backscattered ultrasound from biological tissue is discussed in this chapter. Two types of tissue were investigated, namely; human liver and spleen. The data base gathered for this thesis consisted of five individuals, all of which were assumed to have normal healthy organs.

The rationale behind choosing the liver and spleen organs is two-fold; first, the anatomical placement of both organs is quite similar (i.e. both are adjacent to the abdominal wall), and second, the sono-anatomy of liver is significantly different than that of the spleen. The spleen is quite sono-lucent compared to the liver. The similarities in overlying tissue and differences in acoustic properties of the liver and spleen should facilitate the differentiation between these organs.

The first section of this chapter outlines the data collection procedure and the post processing of collected data. Results obtained from the spectral analysis of liver and spleen echoes are presented in Sections 4.2 and 4.3. Also investigated were the effects of introducing a correction factor (for attenuation due to overlying tissue) to the frequency domain of the transformed tissue echoes. The results of this analysis are contained in Section 4.4.

4.1 BIOLOGICAL TISSUE DATA COLLECTION AND POST PROCESSING

Human liver and spleen data was collected <u>in vivo</u> from five healthy subjects. The procedure is outlined below:

1) The subject was positioned on a firm, horizontal table,

prone for spleen experiments and supine for liver.

2) An acoustic gel was applied to the transducer and to the skin directly above the organ to provide a good acoustic match at the interface.

3) The pulser/receiver was set to maximum energy and damped such that the transducer range for two to three cycles.

4) While monitoring the reconstructed waveform from the A/D converter, the transducer's location and angular orientation were varied so as to achieve proper positioning.

5) Upon locating the proper organ, the subject was requested not to breathe while a single file containing 160 records was taken. A file required approximately five seconds for collection and recording onto the minicomputer's semiconductor memory.

6) The data collected was transfered automatically under software control from semiconductor memory to magnetic tape for post processing.

Backscattered waveforms from the liver and spleen experiments are presented in Figures 4.1 and 4.2. The following criteria were established for determining a time window appropriate for both types of backscattered waveforms.

1) The window must be sufficiently long to minimize spreading in the frequency domain.

2) The window must be sufficiently short to ensure that only the organ of interest contributes to the frequency domain distribution.

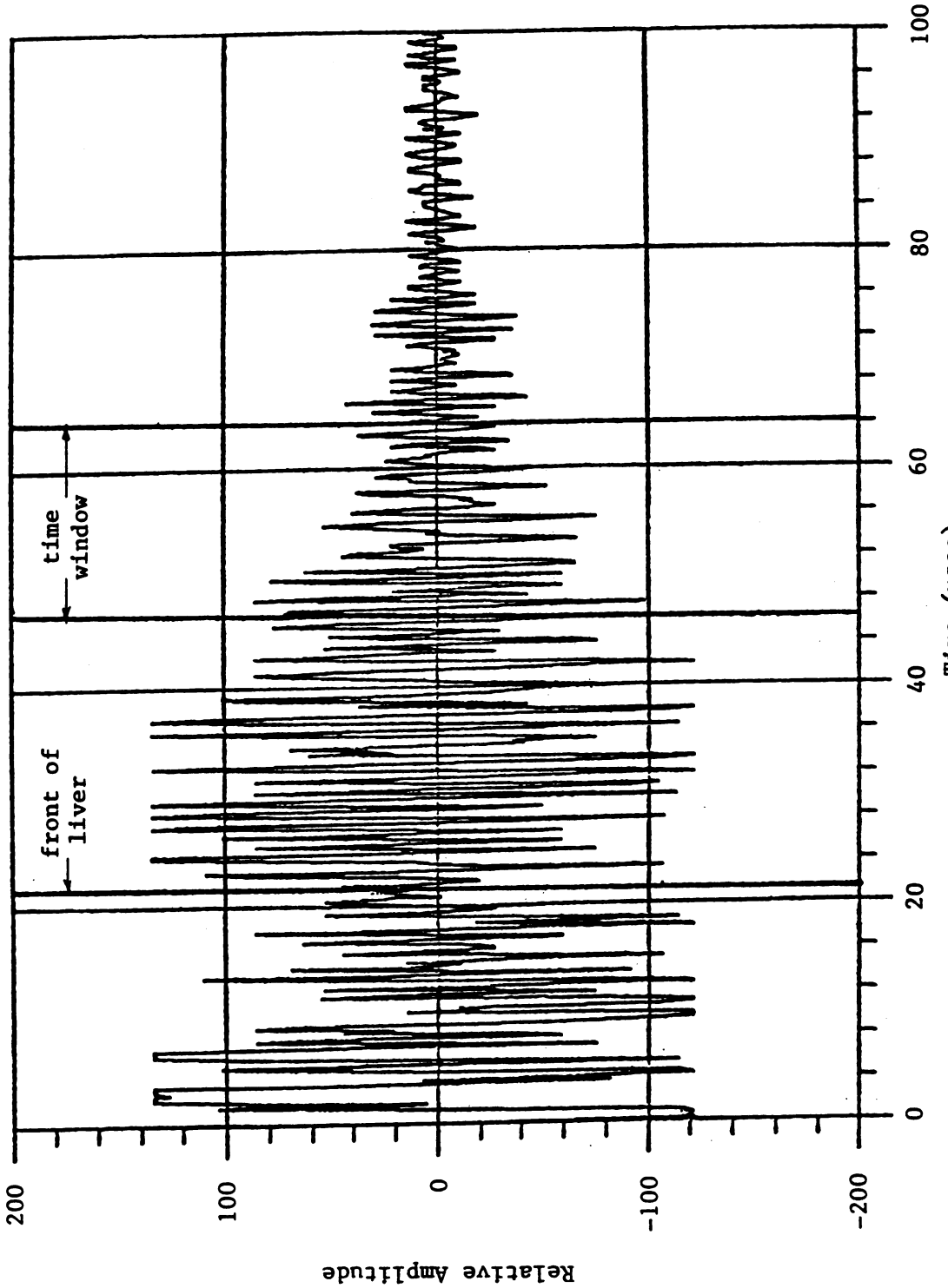

Figure 4.1 Sampled backscattered waveform from liver tissue.

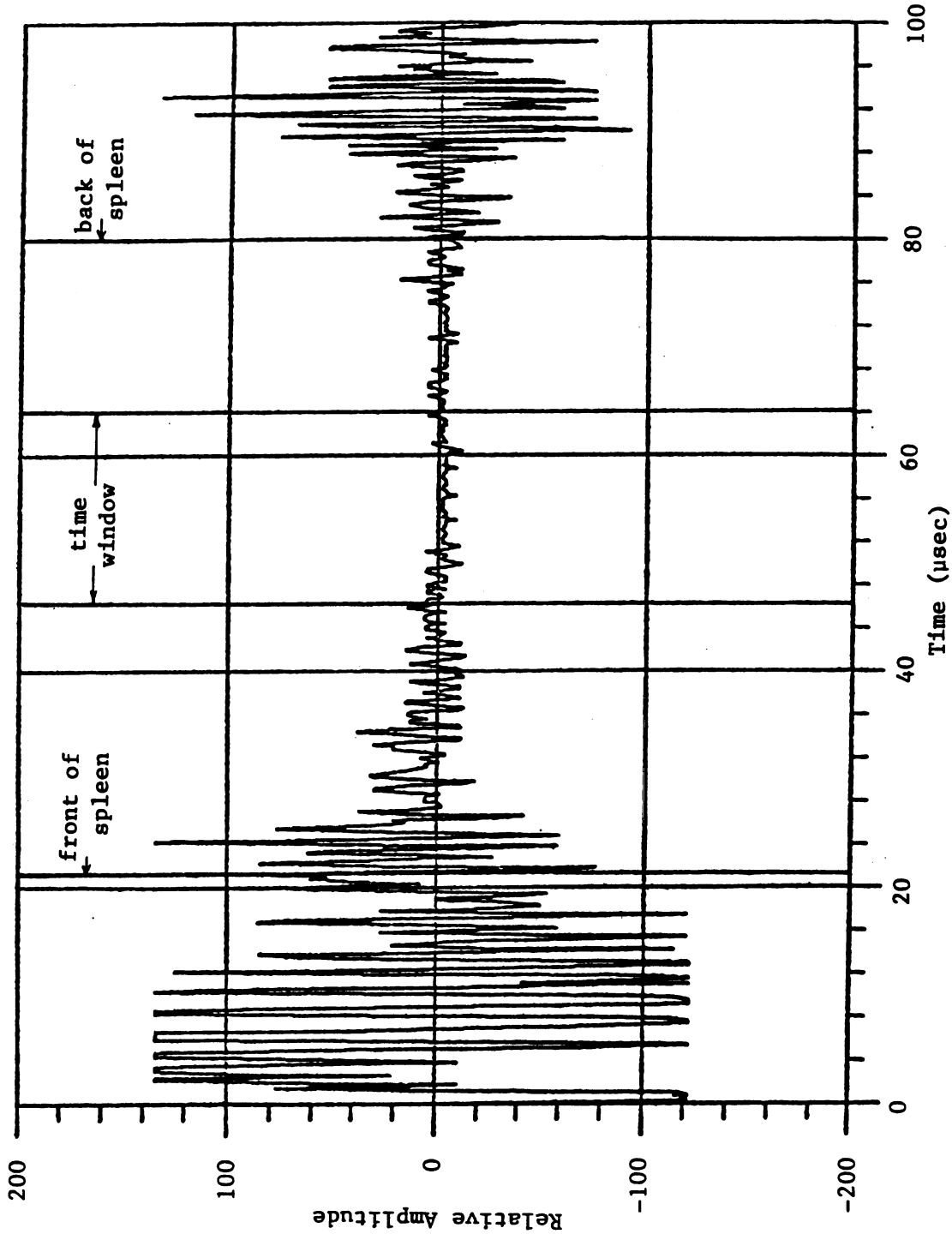

Figure 4.2 Sampled backscattered waveform from spleen tissue.

3) The window must be positioned such that, for a fixed window length determined by 1 and 2 above, the entire window lies within the organ of interest for all subjects.

A window starting position and width that meets all three of the above criteria is indicated in Figures 4.1 and 4.2 by the heavy vertical lines. These lines correspond to a window 18 microseconds long starting 56 microseconds after the transmitted ultrasound pulse was generated. Assuming an average acoustic velocity of 1540 m/second, this window would correspond roughly to a pill box type volume of radius 0.95 cm with a depth of 1.39 cm located 3.54 cm from the abdominal wall/transducer interface (see Figure 4.3). Due to the dispersive nature of the medium and acoustic beam and to the finite temporal width of the ultrasound pulse, the actual interrogated volume does not have such well defined boundaries as indicated by this figure.

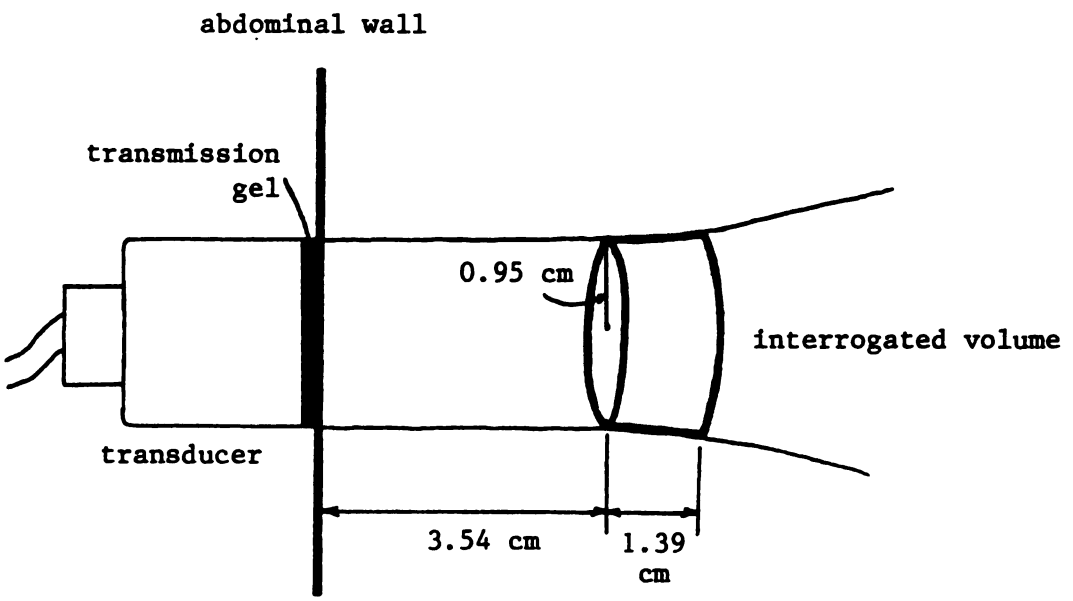

FIGURE 4.3. Interrogated volume defined by time window of Figure 4.1.

A Hanning weighting function was applied to 35 echoes per organ per individual defined by the above time window. The spectral density for each weighted echo was determined, thus establishing two classes, namely; a global liver spectral class, and a global spleen spectral class. The spectrum of Figure 4.1 (member of liver class) is presented in Figure 4.4, while the spectrum of Figure 4.2 (member of spleen class) is presented in Figure 4.5.

Eight statistical measures were calculated for each member of both spectral classes, thus establishing a liver measure matrix and spleen measure matrix. The statistical measures were calculated in the frequency range 0.4 MHz to 1.6 MHz, and are listed here as a reference for the remaining material of this chapter.

M1 - The mean frequency of the spectral density.

M2 - The variance of the spectral density.

M3 - The skewness of the spectral density.

M4 - The Kurtosis of the spectral density.

M5 - The first partial sum (i.e. the ratio of the energy in the range from 0.4 MHz to 0.7 MHz to the energy in the range from 0.4 MHz to 1.6 MHz).

M6 - The second partial sum (0.7 MHz to 1.0 MHz).

M7 - The third partial sum (1.0 MHz to 1.3 MHz).

M8 - The fourth partial sum (1.3 MHz to 1.6 MHz).

4.2 FEATURE SPACE REPRESENTATION

For the purpose of tissue differentiation it would be ideal if a feature space was definable such that tissue classes did not overlap in the space. This is not the case for the feature spaces investigated in this thesis. Consider the feature subspace defined by

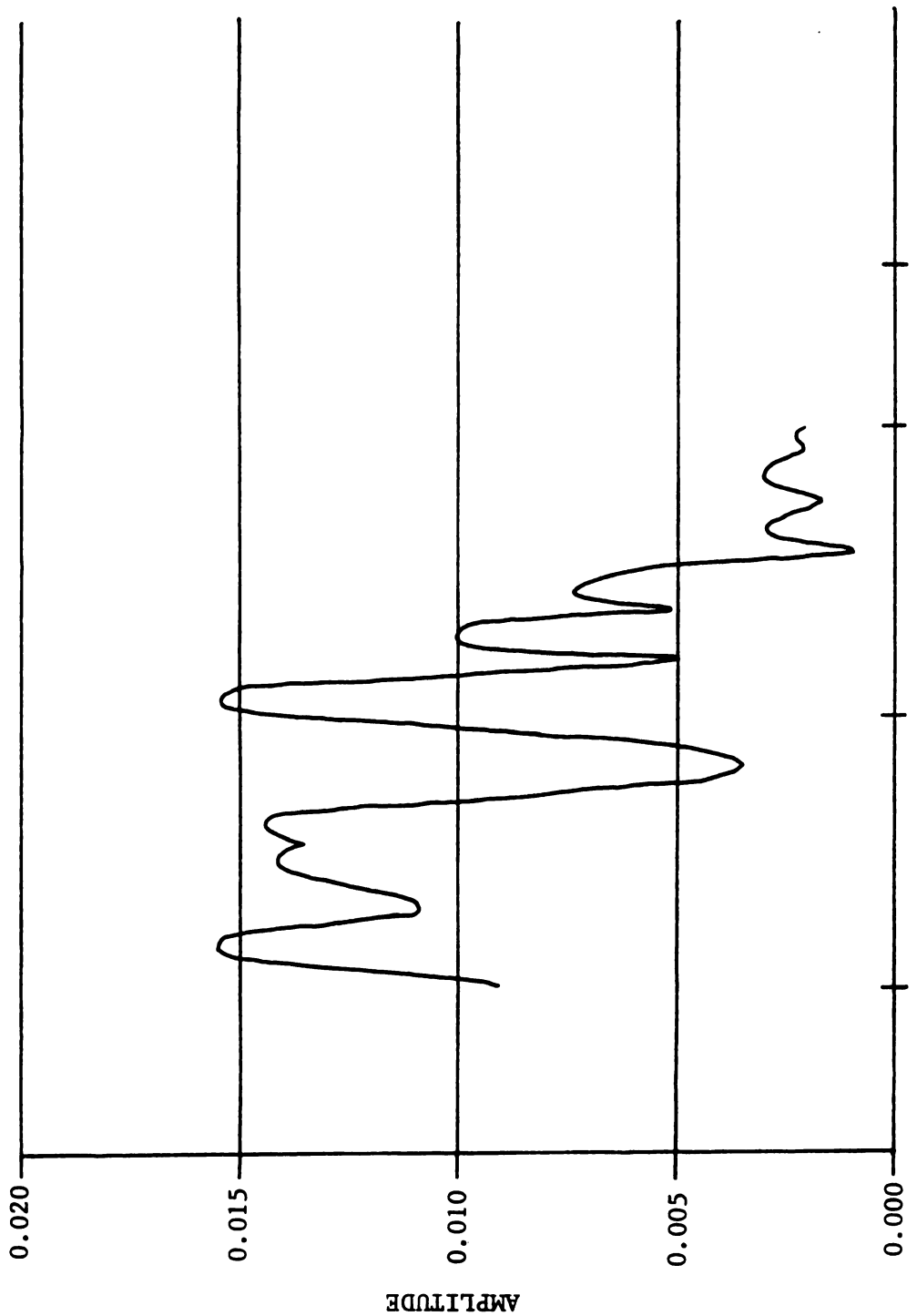

FIGURE 4.4. Normalized Spectrum of backscattered ultrasound from liver tissue (see Figure 4.1).

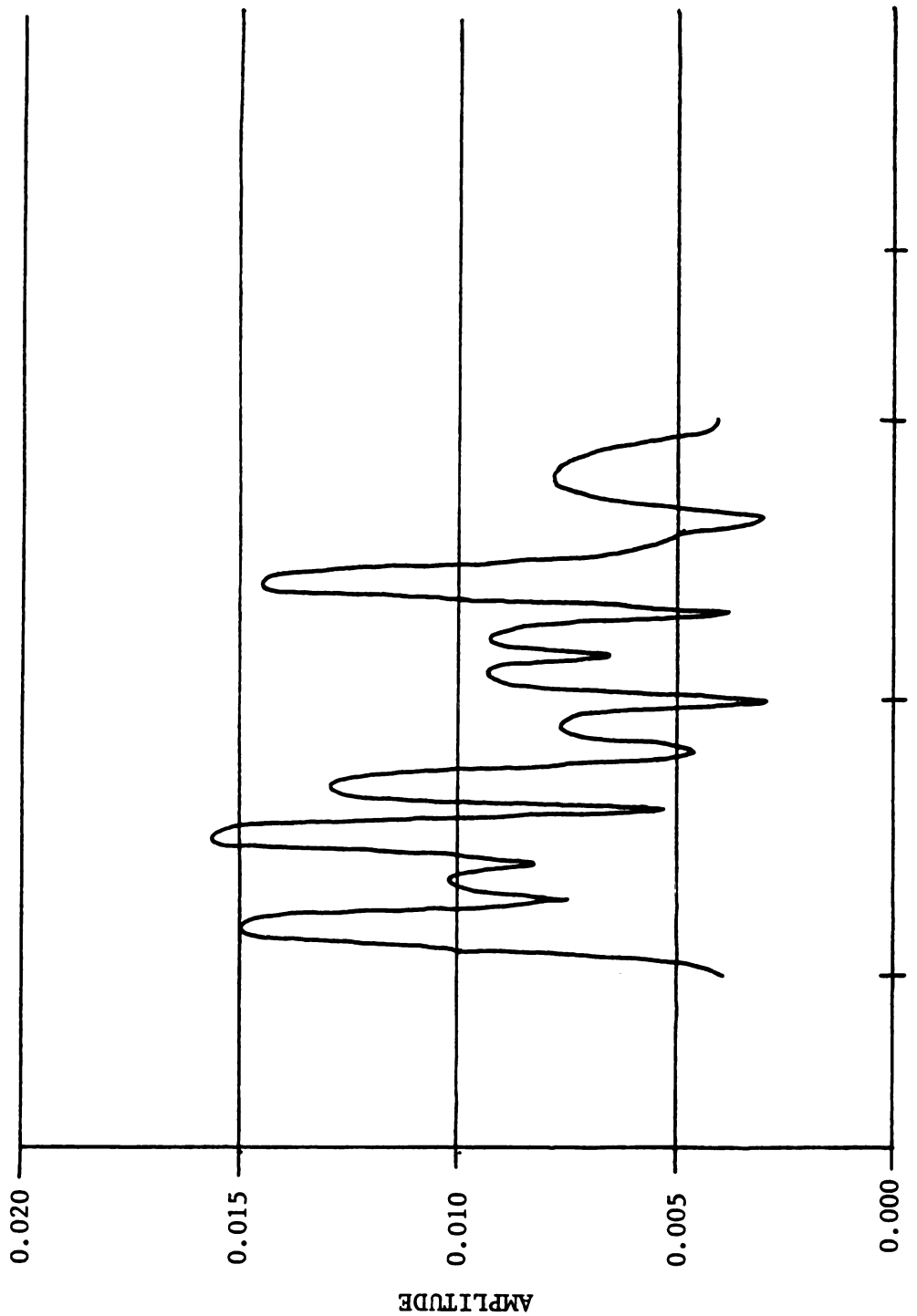

FIGURE 4.5. Normalized spectrum of backscattered ultrasound from spleen tissue (see Figure 4.2).

skewness and kurtosis. A scatter plot of liver and spleen sample points obtained from the spectral and statistical analysis of echoes from one individual is presented in Figure 4.6. Note that although the two centroids of the two classes are distinct the spreads of both classes are sufficiently large to cause an overlap. A scatter plot for all five individuals together with the same two classes, and feature space is presented in Figure 4.7. The overlap in this figure is even more pronounced, to the extent of rendering this approach together with the above feature space virtually useless.

The spread of a class may be attributed to the variation in properties of successive echoes andvariance introduced by different individuals. Variance in the spectra of successive echoes may be attributed to tissue dynamics such as changes in blood pressure and respiration, or to changes in transducer positioning during the course of data collection. Variations due to different individuals may be caused by changes in overlying tissue effects among other things. At any rate, Figures 4.6 and 4.7 indicate that variations due to different individuals tend to be greater than those caused by tissue dynamics and transducer positioning.

Consider first the scatter plot for a single individual (Figure 4.6). A linear boundary has been drawn in this feature space to partition it into two subspaces; one in which a majority of points originate from liver samples, and the other in which a majority of points originate from spleen samples.

The boundary was drawn so as to maximize the total number of sample points in the correct subspace (i.e., liver sample points in liver subspace and spleen sample points in spleen subspace). A success rate may be determined by taking the ratio of organ sample points in the proper subspace to the total number of sample points for that organ in the entire feature space. The success rates for this individual, boundary, and feature space are; liver success rate = 0.76, spleen success rate = 0.83, and total success rate (average of previous two) = 0.80.

Consider next the scatter plot for all five individuals. A piece-wise linear boundary has been drawn in this feature space to partition the liver and spleen classes. Again the boundary was chosen so as to maximize the total number of sample points in the correct subspace. The success rates as defined above are; liver success rate = 0.69, spleen success rate = 0.78, and total success rate = 0.73.

4.3 TISSUE DIFFERENTIATION BY THE MAHLANOBIS METHOD

The method for tissue differentiation demonstrated in the previous section (i.e. drawing the scatter plot and partitioning the feature space) has a few drawbacks. First, the plots are time consuming and tedious. Second, it lacks a certain preciseness in choosing exactly how to partition the feature space. Finally, scatter plots in three dimensions or higher are prohibitively complex to draw. The Mahalanobis

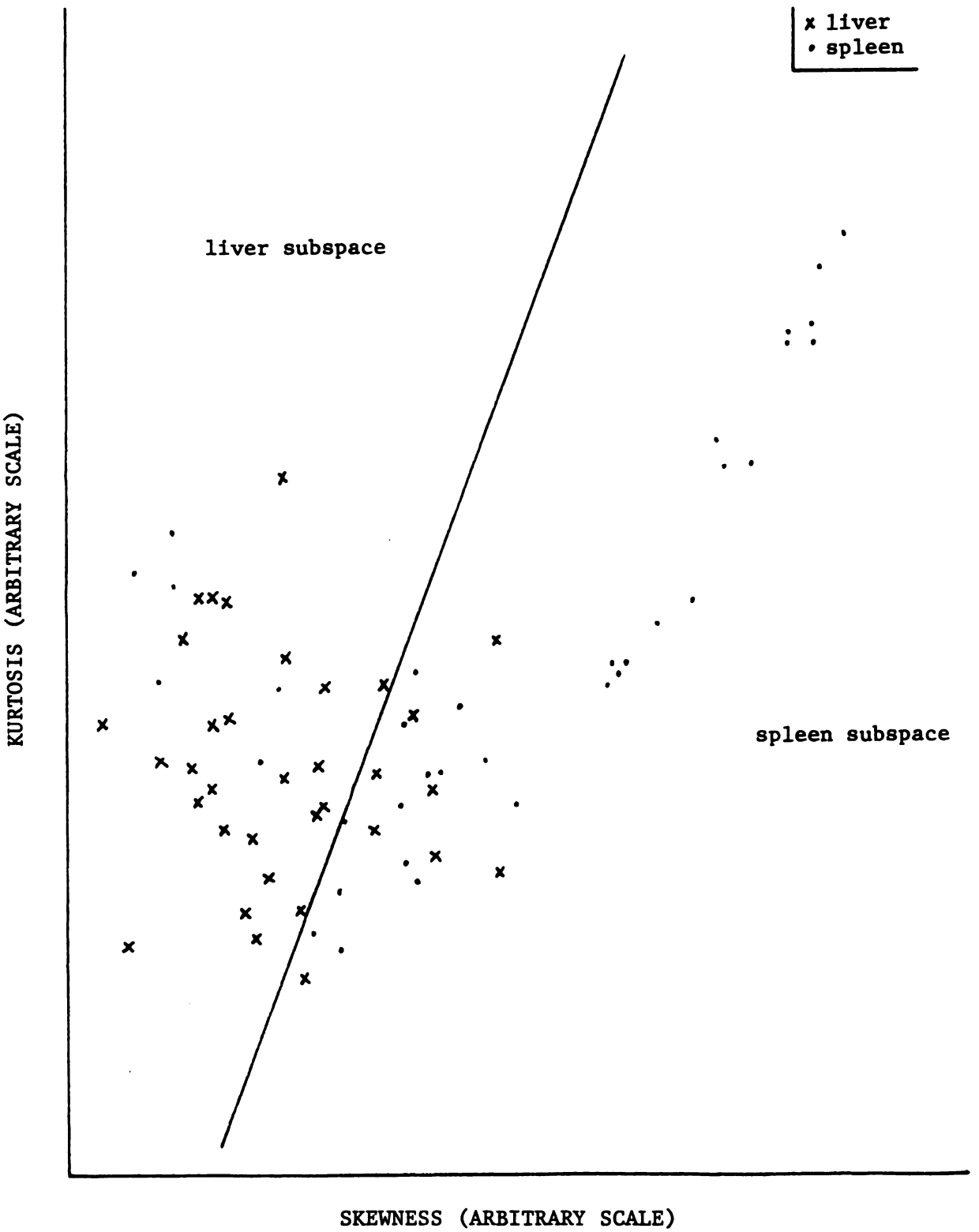

FIGURE 4.6. Scatter plot of liver and spleen samples for a single individual.

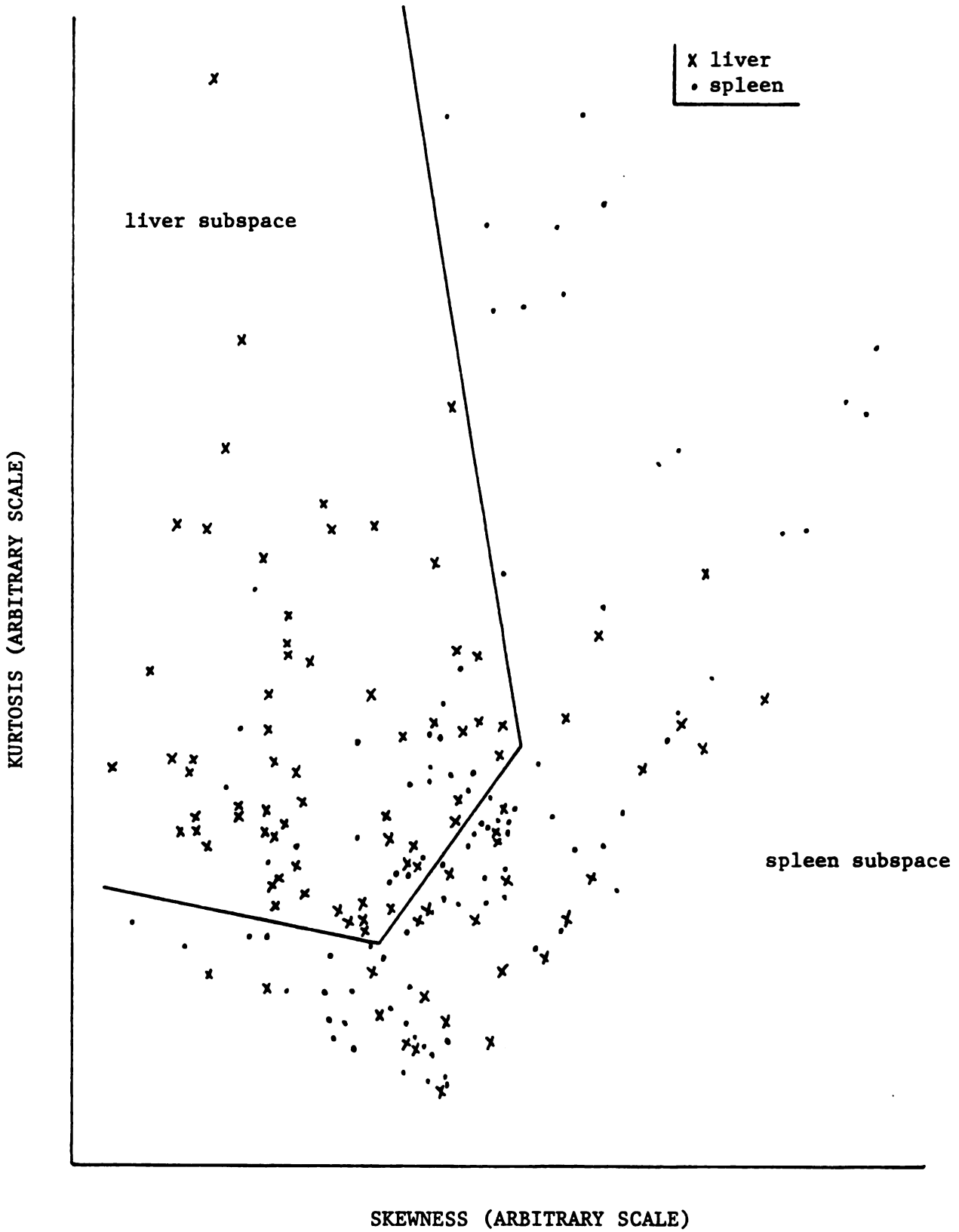

FIGURE 4.7. Scatter plot of liver and spleen samples for five individuals.

method does not suffer these disadvantages, although it does lack a few of the desireable attributes enjoyed by the scatter plot method. For example, the latter method allows one to observe the global relationship of all data points simultaneously whereas the former does not. At any rate, tissue differentiation utilizing the Mahalanobis method has been investigated for all feature subspace defined by combinations of M1 through M8 of order three or less.

The procedure for testing the ability of certain feature spaces to facilitate discrimination of classes through the Mahalonobis method is outlined below.

1) The appropriate columns of the liver and spleen measure matrices were used to define the two classes in the feature space of interest.
2) A sample point was systematically chosen from one of the classes.
3) The entries of the chosen sample point were deleted from the appropriate class matrix (i.e. the class matrix considered the sample point as an unknown).
4) The Mahalanobis distance was calculated from the sample point to the centroid of each class.
5) The sample point was classified as a member of the class to which it lie closest (i.e. its Mahalanobis distance was smallest).
6) Knowing a priori which class the sample point came from, it was noted whether the Mahalanobis method classified the sample correctly or not.

Steps 2 through 6 were repeated for every other member in both spectral classes. Selected results obtained from this testing are presented in Table 4.1. A more comprehensive list is given in Appendix B.

TABLE 4.1

CLASSIFICATION BY MAHALANOBIS DISTANCE

Feature Space	Liver % Correct Calls	Spleen % Correct Calls	Overall % Correct Calls
m2,m3,m4,m6,m7	89.77	64.77	77.27
m2,m3,m4,m6	87.50	65.91	76.91
m2,m4,m7	88.64	62.50	75.57
m2,m4,m6	88.64	56.82	72.73
m1,m2,m4	82.95	61.36	72.16
m3,m4	88.64	53.41	71.03
m6	54.55	64.77	59.66

Results presented in Table 4.1 indicate that liver samples were 'easier' to identify than spleens, except for the M6 feature space. In other words, the measures investigated here were biased toward classifying unknown sample points as members of the liver class. This trend was observed for the vast majority of feature subspace investigated. However, the apparent 'ease' by which a class is called correctly may not be a desireable attribute in and of itself. Consider the feature space, FS, in which a certain class, C_1, is successively differentiated 95% of the time. It is entirely possible for a second

class, C_2, (different from C_1) to also be classified as a member of C_1 95% of the time. In other words, a majority of samples in FS, whether they belong to C_1 or C_2, are classified as members of C_1. Therefore, for classes C_1 and C_2 the feature space, FS, would not facilitate the differentiating between them. This phenomenon has been observed for several feature subspace investigated. For example, the feature space defined by M4 and M5 classified 93.18% of the liver samples and 96.59% of the spleen samples as belonging to the liver sample space.

4.4 INTRODUCTION OF ATTENUATION CORRECTION FACTOR

The analysis of the previous section has been repeated here for the first five feature spaces listed in Table 4.1, with the exception that an attenuation correction factor has been introduced (see Appendix A for details). Two different cases of attenuation due to overlying tissue have been investigated, they are:

1) Attenuation due to overlying tissue was assumed to be the same forboth liver and spleen experiments, and
2) Attenuation due to overlying tissue for liver experiments was assumed to be different than that for spleen.

Case 1.

As a first approximation, an assumed attenuation of 1.24 dB/cm-MHz was introduced for both liver and spleen experiments. This involved multiplying the backscattered spectra by exp (0.143 f d). The factor d is a constant and represents the round trip distance traveled by the ultrasound pulse through the attenuating tissue. The factor f represents the frequency in megahertz. Classification of members from both corrected

spectral classes was performed using the Mahalanobis method and procedure outlined in the previous section. The results are presented in Table 4.2.

Case 2.

As a second approximation, different attenuation factors were assumed for the liver and spleen experiments. Correction for the liver spectral class was the same as in Case 1 (i.e. 1.24 dB/cm - MHz). Consider the backscattered time waveform for spleen samples illustrated in Figure 4.2. In Figure 4.3 the abdominal wall/spleen interface and the position of the time window have been labeled. Note that for the round trip distance from transducer to interrogating volume the ultrasonic pulse must travel through approximately 1.6 cm of abdominal wall tissue and 1.9 cm of spleen tissue. Attenuation due to spleen tissue was assumed to be relatively small compared to the liver as evidenced by the strong reflections originating from behind the spleen. Therefore, for Case 2, the overlying tissue attenuation for spleen was taken to be 1.14 dB/cm - MHz.[†]

In general, an across the board application of an attenuation correction factor (see Case 1) did not tend to increase the success rate of the classifier, while selectively applying an attenuation correction factor did (see Case 2). In either case, the changes in marginal success rates were not great, except for feature space (M1, M2,M4). For this feature space a significant decline in the liver success rate was accompanied by a significant rise in the spleen success

[†]There is a lack of published data on attenuation for *in vivo* spleen. The value 1.14 dBcm MHz used for Case 2 spleen is rather arbitrarily chosen.

rate. Overall, the total success rate did not change drastically for either Case 1 or Case 2 and all feature spaces considered.

TABLE 4.2

CLASSIFICATION BY MAHALANOBIS DISTANCE

ATTENUATION INTRODUCED*

Feature Space	Liver % Correct Calls	Spleen % Correct Calls	Overall % Correct Calls
m2,m3,m4,m6,m7	90.91 (92.05)	62.50 (65.91)	76.71 (78.98)
m2,m3,m4,m6	87.50 (90.91)	60.23 (64.77)	73.87 (77.84)
m2,m4,m7	89.77 (89.77)	51.14 (52.27)	70.46 (71.02)
m2,m4,m6	92.05 (93.18)	53.41 (56.82)	72.73 (75.00)
m1,m2,m4	75.00 (77.27)	68.18 (69.32)	71.59 (73.30)

*The numbers in parenthesis correspond to Case 2 results.

CHAPTER V

CONCLUSION

The spectral distribution or backscattered ultrasound from biological tissue has been investigated. The motivation for this study has been the prospect of determining a set of discriminant features that would facilitate differentiation between tissue classes. Also investigated were the effects of applying a correction factor accounting for attenuation due to overlying tissue to the spectral distributions of backscattered diffuse echoes.

The biological tissues investigated were human liver and spleen. The experiments were performed in vivo on five subjects, all of which were assumed to have normal healthy organs. The spleen and liver were chosen for two reasons. First, the type of overlying tissue and propogation distances through this tissue were similar for both liver and spleen examinations (i.e. the overlying tissue was approximately 2 cm deep and consisted primarily of fat and muscle tissue). This de-emphasized but did not eliminate variations between in vivo liver and spleen spectra that were not intrinsic to the organs themselves. Second, as reported in the literature[19,20] the liver and spleen possess significantly different sonoanatomies, thus facilitating discrimination between them based on properties of the organ.

The spectral distributions of diffuse echoes recorded for both liver and spleen organs were determined using a Fast Fourier Transform (FFT). Prior to transformation, a Hanning weighting function was applied to a time window corresponding to diffuse echoes originating

from the organ of interest. This weighting function suppressed sidelopes in the frequency domain introduced by time limiting the backscattered waveform. To characterize the backscattered echoes eight statistical measures of the spectral distribution were determined; they were, the mean frequency, variance, skewness, kurtosis, and first through fourth partial sums. All measures were defined on the frequency range 0.4 MHz to 1.6 MHz.

Two methods for tissue classification were investigated; namely, the scatter plot method and Mahalanobis method. These classifiers were applied to feature spaces defined by subsets of the statistical measures listed above. The Mahalanobis method was applied to all feature spaces of order three or less. In addition, a few higher order feature spaces were investigated. A scatter plot was drawn for the two dimensional feature space in which the Mahalanobis method performed best. Additional scatter plots have also been investigated but were not presented, however, they exhibited similar results as those observed forthe scatter plot presented in Section 4.2.

The scatter plot method was useful in gaining insight into the sources of difficulty associated with differentiating between tissue classes using the features chosen in this study. A few observations are listed below.

1. The feature spaces that were investigated using the scatter plot method exhibitted varrying degrees of overlap between the classes.
2. Class overlap was more extensive when considering a group of subjects as opposed to a single individual.

3. For a single individual a linear boundry was sufficient to seperate the tissue classes while maintaining an overall success rate above 0.80.
4. A piece-wise linear boundary was required for scatter plots in which all five subjects were considered to maintain an overall success rate above 0.70.

The above observations are related to the variance and close proximity of the tissue classes. The variance associated with an individual may be attributed to tissue dynamics (e.g., blood pressure or respiration), or alternations in transducer position during data collection, or noise introduced by the data collection system (e.g., quantization error by A/D). Variance associated with a group may be attributed to such things as varying properties of overlying tissue between individuals (e.g., more fat than muscle contributing to the overlying tissue), or basic differences in the properties of the investigated organs (e.g., density or compressibility variations of the tissue). Close proximity of the tissue classes may be attributed to a moderate sensitivity of the discriminate features to liver andspleen tissue and/or similar tissue signatures for both liver and spleen organs.

As stated above, moderate success rates (>0.70) could be achieved using the scatter plot method for both single individual and group tissue classes. However, the success rates for group classes were noticeably less than those for a single individual, as expected, due to additional variance introduced by the group. This suggests that for much larger groups this method may prove less useful for tissue differentiation. An alternative approach may be to consider only one individual at a time.

For example, consider the problem of diagnosing the pathology of a portion of a patient's liver. Most likely this type of differentiation would be much more difficult than liver/spleen differentiation due to the subtlety of the tissue variations than that considered in this research. At any rate, one may approach this task by attempting to establish a 'normal' liver tissue class from analysis of a portion of the organ known to be healthy (e.g., the left lobe if the right lobe is suspected of being deseased). Comparison of echo analysis results from the suspected deseased tissue with those from the 'normal' class may reveal the pathology of the suspect isssue, assuming a good set of differentiating features could be established.

The Mahalanobis distance provided a faster, more precise method for classifying tissue samples than the scatter plots. A few observations from the results of theMahalanobis method are listed below (the liver and spleen tissue classes considered were those that accounted for all five subjects).

1. For feature spaces of order three or less the overall success rate never exceeded 0.76.
2. The liver success rates were almost always greater than the spleen success rates.
3. In general, the higher the order of the feature space the better the success rate was, however, the success rate did not increase significantly as the order increased.

The success rates using the Mahalanobis method and the feature space defined by the skewness and kurtosis agreed relatively well with that determined by the scatter plot method. The overall success rates

for these two methods were 0.71 and 0.73 respectively.

The Mahalanobis method has also been applied to tissue classes for which a correction factor accounting for attenuation due to overlying tissue has been applied. It was found that an across the board application of an approximately determined correction factor did not improve the effectiveness of the classifier. Instead, a slight decrease in success rates was observed. Conversely, when a correction factor reflecting the difference in attenuation due to overlying tissue for liver and spleen echoes was applied a slight increase in success rates was observed. The approach used in this study for applying correction factors intended to offset effects due to overlying tissue has not been very rigorous, although results obtained indicate that a more precise application of correction factors may prove very usefull in increasing the effectiveness the classifiers studied. Methods for determining attenuation factors have been established for in vivo experiments and are relatively accurate. Application of these methods to the classifier and feature spaces considered here should prove interesting.

The research conducted for this thesis has been preliminary in nature. That is, the main objective has been to determine a set of discriminating features that could be used for discerning tissue class. In addition, the effects of overlying issue have been addressed. Results generated from the spectral analysis of backscattered radiation are encouraging and warrent further research into the tissue differentiation methods presented in this thesis.

The application of a more exact measure of the attenuation coefficient for overlying tissue should prove useful in increasing the effectiveness of the discriminatory features. Experiments performed

in vitro are more appropriate for estimation of attenuation correction factors than in vivo. For example, consider the task of classifying the state (e.g., fresh, frozen, fixed, etc.) of excised porcine liver. If one were to analyze diffuse echoes from anywhere except directly beneath the water/liver interface there would be attenuation of the backscattered radiation due to overlying liver tissues. The attenuation coefficient may be determined by the following procedure.

With a suspended sample of porcine liver above a thick metal block (block normal to ultrasound beam) execute a B-mode scon of the tissue (i.e., spatially sweep the transducer across the liver while pulsing and receiving at intermediate stationary positions). Determine the round trip distance through the tissue for each intermediate position at which data was taken. After removing the liver specimen collect backscatter echoes from the metal block with no intervening tissue over an area that was covered by the B-mode scan. The ratio of the spectral distribution determined from the backscattered echo originating from the metal block's front surface with intervening tissue to that without yields the attenuation. Dividing the above attenuation by the round trip distance through the tissue will yeild the attenuation coefficient (α) as a function of frequency with units of inverse centimeters. Application of this factor on an echo by echo basis to the backscattered spectral distribution should eliminate the affect of overlying tissue on the discrimination problem. Also it would be instructive to experimentally study feature subset properties for various known reflectors, such as planes, thin cylinders, and point like reflectors. Such further work should contribute to an appreciation of the relative role of the various contributors to quantitative measures of backscattered ultrasound,

and is imperative to the optimum application of tissue signature techniques.

APPENDICES

APPENDIX A

The postprocessing and analysis of backscattered ultrasound from various reflectors is performed with the aid of two interactive Fortran programs; namely, PLOTS3 and FTRS3. The following sections outline the usage of these programs.

A.1 PLOTS3 DOCUMENTATION

PLOTS3 must be run from the TEKTRONIX graphics terminal. The user requests tasks to be run via 2 letter mnemonic commands, which are input when the '$' prompt appears on the terminal. Most tasks require additional input, these are discussed below. If an illegal command or input is entered the program will request the input again. The following is a list of commands and the associated tasks.

MNEMONIC	NAME	SECTION	TASK
RD	READ	A.1.1	Reads ultrasound data from user specified disk file.
PL	PLOT ULTRASOUND DATA	A.1.2	Plots ultrasound data as continuous waveform as a function of sample interval.
FT	FAST FOURIER TRANSFORM	A.1.3	Performs an FFT on user specified weighted sample window.
PS	POWER SPECTRUM	A.1.4	Calculates the power spectrum (amplitude squared) from FFT reslts.
RT	SPECTRA RATIO	A.1.5	Determines the ratio between two discrete frequency spectra (i.e., deconvolution).
NR	NORMALIZE FREQUENCY SPECTRUM	A.1.6	Normalizes the sum of the spectral components in a specified frequency range to unity.

MNEMONIC	NAME	SECTION	TASK
AT	ATTENUATION CORRECTION FACTOR	A.1.7	Applies a user specified attenuation correction factor to the frequency spectrum.
PF	PLOT FREQUENCY	A.1.8	Plots frequency spectrum.
MD	MINIDRIVER	A.1.9	Calculates statistical measures of the spectral distribution for a user specified set of ultrasound records and stores results on disk file.
ST	STOP	——	Terminates PLOTS3

PLOTS3 exists on the third partition of the ultrasound disk. To start execution of the program enter the following input at the graphics terminal;

```
;SCHED,PLOTS3,p,ww
```

where

p = priority (usually 5)

ww = logical unit number of the third partition of the removable platter drive in which the ultrasound disk has been placed.

The following output will appear at the graphics terminal;

```
INPUT FILE #'S OF ULTRASOUND DISK
F1 F2
xx yy
```

where

xx = user input indicating the second partition of the ultrasound disk,

and yy = user input indicating the third partition of the ultrasound disk.

If disk drive D013 is used, ww = 26, xx = 25, and yy = 26.

A.1.1 READ

The following sequence of inputs will instruct the program to read an ultrasound data record from a disk file. Outputs to the terminal are signified by upper case characters, inputs by the user are signified by lower case characters.

```
$rd
FILE NAME AND DATA TYPE (1 numerator, 2 denominator)
NNNNNN T
nnnnnn t
```

where

nnnnnn = name of data file. There are six data files that currently exist on the ultrasound disk. They are ULTRA1 through ULTRA6.

and t = 1 or 2 as indicated above. This input is used to flag the spectral distribution associated with the ultrasound data when a ratio between distributions is requested. See RT command.

```
RECORD NUMBER
NNN
nnn
```

where

nnn = the number of the record that is to be read from the ultrasound file. This number must lie between 2 and 160.

```
DOES THIS FILE HAVE A HEADER? (T OR F)
X
x
```

If the file does have a header it will be output following a 'T' input.

where

x = T if the file does have a header, and F if the file does not have a header.

```
ENTER START OF WAVE ARRAY
ISTR
ssss
```

where

ssss = Each data record contains 2048 words of of data. Only 1024 of these words are stored into the programs common memory to conserve on memory space. It is therefore necessary to indicate where the first word of the 1024 block should start in the 2048 block. 'ssss' should never exceed 1024.

A.1.2 PLOT ULTRASOUND DATA

The following inputs will instruct the program to plot the raw ultrasound data previously read. This task allows the user to choose an appropriate time window by displaying the backscattered waveform. The

horizontal axis is directly proportional to time. To determine the corresponding time, multiply the horizontal axis number by the appropriate sampling period (in most cases this should be 0.2 μsec.). The user should be aware of the implicit sample (or time) offset introduce by reading only a portion of the data record as mentioned above (i.e., if ssss = 10, then 1 on the horizontal axis corresponds to the 10th sample).

```
$pl
INPUT LAST ARRAY POS. TO PLOT
LLLL
1111
```

where

1111 = the last sample point in the ultrasound data to be plotted. This number must be less than 1024.

A.1.3 FAST FOURIER TRANSFORM

The user may request that an FFT be calculated for any specified sequence of sample points less than 512 words long. Before calculating the FFT a user specified weighting function is applied to the sequence of data points and zero filled so that the FFT always calculates the spectral components for a time sequence 512 words long. The following inputs and outputs are associated with an FT command.

```
$ft
  ENTER WORD RANGE OF TIME WINDOW
  WFWD WSWD
  xxxx yyyy
```

where

xxxx = the first sample point of the window (this is the offset value on the raw data plot).

yyyy = the last sample point of the window (this also is the offset value on the raw data plot).

```
YOUR CHOICES OF WINDOW FUNCTIONS ARE:
     FUNCTION     CODE
     HANNING       01
     HAMMING       02
     TRIANGULAR    03
     BLACKMAN      04
     RECTANGULAR   05
ENTER CODE OF WINDOW FUNCTION --
cc
```

---

where

cc = 01 through 05. Note that the weighting function code must not be preceeded by any blank spaces. If an illegal code is entered the rectangular weighting will be used.

```
ENTER NORMALIZED FREQUENCY RANGE.
F.1 F.2
xxx yyy
```

---

where

xxx = the lowest frequency component of interest. This number must be a real number and is rounded off to the tenths position. The frequency is assumed to be in MHz.

yyy = the highest frequency component of interest. This number must also follow the guide lines as xxx.

The above inputs are all that is necessary. A typical output as shown below will follow the last input.

```
FRSTF -    .39   SCNDF -   1.60
WINDOW TYPE USED: HANNING
     MEAN FREQUENCY =    .823     FIRST PARTIAL SUM =  .400
 STANDARD DEVIATION =    .301    SECOND PARTIAL SUM =  .283
           SKEWNESS =    .500     THIRD PARTIAL SUM =  .243
             EXCESS =   2.34    FOURTH PARTIAL SUM =  .740E-01
```

FRSTF is the lowest frequency considered and SCNDF is the highest frequency considered.

A.1.4 POWER SPECTRUM

The power spectrum is calculated by squaring the results of an FFT. The inputs and outputs are indentical to those presented in section A.1.3.

A.1.5 SPECTRA RATIO

The ratio between two spectral distributions may be calculated. This operation corresponds to deconvolving the two associated time domain sampled waveforms. Before a ratio may be requested the following tasks must be performed.

1) read an ultrasound data record and flag the data as the numerator (i.e., data type = 1),

2) request either an FT or PS,

3) read another ultrasound data record and flag the data as the denominator (i.e., data type = 2),

4) request the same task as in 2 with the same parameters (e.g., same time window, weighting function, etc.).

The following is an example of an RT command.

```
$rt
 STATISTICS ARE PERFORMED ON RATIO OF NORMALIZED
 DATA IN THE FREQUENCY RANGE    .4 TO 1.6
 WINDOW TYPE USED: HANNING
      MEAN FREQUENCY =    .994    FIRST PARTIAL SUM =    .244
  STANDARD DEVIATION =    .354   SECOND PARTIAL SUM =    .246
            SKEWNESS = -.256E-1 THIRD PARTIAL SUM =    .243
              EXCESS =   1.79   FOURTH PARTIAL SUM =    .267
```

A.1.6 NORMALIZE FREQUENCY SPECTRUM

After any spectral distribution has been calculated the user may request that the results be normalized. Normalization of all spectral lines in the frequency range specified by the user in the previous FT or PS command sequence will be performed as follows;

1) all spectral components in the specified frequency range are summed,

2) the result of step 1 is divided into each spectral component of the specified frequency range.

The results are stored in the same array that the original spectral distribution existed in.

A.1.7 ATTENUATION CORRECTION FACTOR

An attenuation correction factor of the form exp(αd) may be applied to the frequency domain to offset effects of overlying tissue. The user must specify the attenuation per centimeter per megahertz, the acoustic velocity of the overlying tissue, and the first sample point that corresponds to the beginning of the overlying tissue. The AT command is as follows. This command must preceed an FT command.

```
$at
ATTEN. COEFF. (DB/CM MHZ), VELOCITY (M/SEC) AND FIRST POSITION OF TARGET
ATTEN VELOCITY FRST
aaaaa vvvvvvvv ffff
```

where

aaaaa = attenuation coefficient with units of db/cm·MHz,

vvvvvvvv = the velocity of sound in the overlying tissue, this number must be real and have units of meters/sec.,

ffff = the first sample point corresponding to the beginning of the overlying tissue.

A.1.8 PLOT FREQUENCY

The following input instructs the program to plot the calculated frequency distribution. The spectrum is plotted only in the frequency range specified by the user previously.

```
$pf
```

A.1.9 MINIDRIVER

The MD command allows the user to analyze a set of backscattered echoes from the same class and store the results onto disk file with a minimum requirement of user inputs. The following sequence of inputs are necessary for the minidriver task.

```
$md
ENTER FILE NAME --
NNNNNN
nnnnnn       (see section A.1.1)
ENTER WORD RANGE --
WFWD WSWD
xxxx yyyy    (see section A.1.3)
ENTER WINDOW CHOICE --
WC
cc           (see section A.1.3)
ENTER FREQUENCY RANGE --
F.1 F.2
xxx yyy      (see sectiom A.1.3)
ENTER START OF WAVE ARRAY --
ISTR
ssss         (see section A.1.1)
ENTER FILE TO BE WRITTEN ON (1-SAVSTT 2-SAVSTS)
F
f
```

There are two files (SAVSTT and SAVSTS) that exist on the ultrasound disk that were explicitly created for this purpose. In additon there are two other files (SAVSTA and SAVSTB) that may be used for storing this type of data. The user may use the graphics editor to transfer data from the former two files to the later two files.

```
ENTER RECORD INCREMENT --
IN
ii
ENTER NUMBER OF RECORDS --
NR
nn
```

---

where

ii = the increment by which records will be read (e.g., if ii = 5, then the 2nd, 7th, 12th, etc. records will be analyzed).

nn = the number of records to be read and analyzed.

After entering the last input the program will execute the following set of tasks without further user inputs.

1) Execute an RD task for the appropriate record and file as specified above.

2) Execute an FT task.

3) Store all calculated statistical results onto the appropriate file as specified above.

Typically MD is used to obtain a set of statistical measure for a class

that may be used to test the effectiveness of the measures coupled with a classification technique to discriminate between classes.

A.2 FTRS3 DOCUMENTATION

FTRS3 should be run on the TEKTRONIX graphics terminal. To start execution of the program enter the following input;

```
;SCHED,FTRS3,p,ww
```

where

p = priority (usually 5),

and ww = logical unit number of the fourth partition of the ultrasound disk. If disk drive D013 is used then ww = 27.

The following sequence of outputs and appropriate inputs should follow.

```
DATA FILES ARE ON?  ---- SAVSTT & SAVSTS --1, OR SAVSTA & SAVSTB --2
r
```

where

r = 1 if the sets of statistical measures are stored on SAVSTT and SAVSTS, or 2 if the sets of statistical measures are stored on SAVSTA and SAVSTB. Note that the user's responce is typed in column 1.

```
# OF RECORDS IN SAVSTT AND SAVSTS (or SAVSTA AND SAVSTB)?
FTT FTS
xxx xxx
```

where

xxx = the number of data records in SAVSTT or SAVSTA,

and yyy = the number of data records in SAVSTS or SAVSTB.

```
INPUT NUMBER OF DATA BLOCKS (AS DEFINED BY FTT ABOVE)
TO SKIP ON INPUT FILE.
NUM
nnn
```

where

nnn = an integer number of data blocks to skip. A data block is defined as the number of input records specified by FTT. By using various combinations of FTT and NUM the user may access different blocks of data from both input files.

```
 Do you wish the statistics and covariance matrix printed out? (T or F)
r
```

where

r = T for true or yes, and F for false or no. If a T is entered the statistics and covariance matrix are printed out on the line printer.

```
 Do you wish to classify a group of points? (T or F)
r
```

where

r = T for yes and F for no.

If a group of sample test points are not to be classified the following sequence of outputs and appropriate inputs should follow.

```
 ENTER SAMPLE #, SAMPLE FILE, AND FEATURE SPACE (1-SAVSTT 2-SAVSTS)
 NUM S S
 nnn x y
```

where

nnn = record number from sample file that is to be tested against the set of records in the feature space,

x = 1 if the sample file (i.e., the file from which the sample record is taken) is SAVSTT or SAVSTA, and 2 if the sample file is SAVSTS or SAVSTB,

y = 1 if the feature space (i.e., the file that the sample record is tested against) is file SAVSTT or SAVSTA, and 2 if the feature space is file SAVSTS or SAVSTB.

A set of feature vectors will be request at this point. The user may enter as many as 10 seperate feature vectors. The following example illustrates the input of a set of feature vectors.

```
ENTER FEATURE VECTOR
F1 F2 F3 F4 F5 F6 F7 F8
a1 a2 a3 a4 a5 a6 a7 a8
ENTER FEATURE VECTOR
F1 F2 F3 F4 F5 F6 F7 F8
b1 b2 b3 b4 b5 b6 b7 b8
.
.
.
ENTER FEATURE VECTOR
F1 F2 F3 F4 F5 F6 F7 F8
no entries (i.e., a return with no numbers inputted is entered, this
terminates the request for additional feature vectors)
```

where

a1 - a8 any combination of 01 through 08.

b1 - b8 = 01 - mean 05 - first partial sum
... 02 - variance 06 - second partial sum
03 - skewness 07 - third partial sum
04 - kurtosis 08 - fourth partial sum
Note that if 10 feature vectors are entered the program will automatically terminate additional requests for feature vectors, and proceed with previously entered set of feature vectors.

After completion of the feature vector inputs the program will calculate the Mahalanobis distance between the test point (indicated by the specified sample file and record number) and centroid of the feature space file. A sample output is presented below.

```
                .278130E-07
MAHAL DSTN  =  5.722      1 2 3 0 0 0 0 0        FSPACE = 1
                                                 SSPACE = 1    SNUM = 3
```

The first number is the determinate of the covariance matrix. The validity of the output is suspect if this number is a few orders of magnitude less than that shown here,for this indicates that the matrix is becoming singular and the method for determining the inverse fails. The number after 'MAHAL DSTN' is the calculated Mahalanobis distance between the test point and feature space class centroid. The eight integers

following this number are the feature components used for the calculations. FSPACE is the file that was specified for the feature space and SSPACE and SNUM are the file and record number used as the test point. After outputing the results for all feature vectors requested the progtam will loop back to the request for a change of feature vector. The program then continues from this point as described above.

If a group of sample test points are to be classified the following sequence of outputs and appropriate inputs should follow.

```
INPUT # OF SAMPLES, INCREMENT, AND SAMPLE SPACE
NUM IN S
nnn ii s
```

where

nnn = the number of samples to be classified using the least Mahalanobis distance method,

ii = the increment by which the test points are to be taken from the sample space file,

s = 1 if the sample space file is SAVSTT or SAVSTA, and 2 if the sample space file is SAVSTS or SAVSTB.

The above input performs the following task;

1) Determine which record is to be used for the test point.
2) Delete this record from the appropriate file.
3) Calculate the Mahalanobis distance from this test point to the centroids of both input files.
4) If specified, tally the number of correct classifications obtained.
5) Loop back to 1 until all test points as specified by nnn above have been classified.

The user may specify that either the results of all distance calculations be outputted to the line printer or that just the percentage of correct classifications be outputted to the graphics terminal. Results printed on the line printer are formatted the same as described on the preceeding page for all distance calcualtions. The following is an example of the output of the percentage.

SAMPLE SPACE IS 1 AND % OF CORRECT CALLS WAS 83.33

where

SAMPLE SPACE = 1 if the test points came from SAVSTT or SAVSTA, and 2 if the test points came from SAVSTS or SAVSTB.

After classifying all test points the program loops back to the request for if the statistics and covariance matrix should be printed out. The program proceeds as before from this point. The program may be terminated by sending two returns in a row to the computer.

APPENDIX B

The success rates for all feature spaces of order three or less have been determined using the Mahalanobis method and procedure outlined in Section 3 - for liver and spleen tissue classes. These classes contained 35 samples per organ per subject. There were five subjects, thus each tissue class contained 185 feature vectors. The components of the feature spaces were chosen from the following list of measures determined from the backscatter tissue spectra.

MEASURE*	MNEMONIC
MEAN FREQUENCY	M1
VARIANCE	M2
SKEWNESS	M3
KURTOSIS	M4
FIRST PARTIAL SUM	M5
SECOND PARTIAL SUM	M6
THIRD PARTIAL SUM	M7
FOURTH PARTIAL SUM	M8

* All measures were calculated in the frequency range 0.4 MHz to 1.6 MHz

The following table presents the results obtained. The first column lists the mnemonics for the feature space components, the second and third columns list the marginal success rates for the liver and spleen classes respectively, and the fourth column is the total success rate for that feature space (average of columns 2 and 3).

TABLE B.1

SUCCESS RATES USING MAHALANOBIS METHOD

Feature Space	Liver Success Rate	Spleen Success Rate	Total Success Rate
M1	.511	.580	.546
M2	.568	.602	.585
M3	.580	.648	.614
M4	.977	.057	.517
M5	.921	.182	.551
M6	.546	.648	.600
M7	.693	.409	.551
M8	.591	.534	.563
M1 M2	.648	.602	.625
M1 M3	.625	.591	.608
M1 M4	.830	.375	.602
M1 M5	.784	.546	.665
M1 M6	.739	.523	.631
M1 M7	.648	.523	.585
M1 M8	.648	.466	.557
M2 M3	.636	.705	.671
M2 M4	.841	.557	.699
M2 M5	.705	.557	.631
M2 M6	.784	.557	.671
M2 M7	.727	.580	.653
M2 M8	.682	.602	.642
M3 M4	.886	.534	.710
M3 M5	.716	.557	.636
M3 M6	.716	.580	.648
M3 M7	.716	.557	.636
M3 M8	.568	.682	.625
M4 M5	.932	.034	.483
M4 M6	.830	.455	.642
M4 M7	.943	.205	.574

Feature Space	Liver Success Rate	Spleen Success Rate	Total Success Rate
M4 M8	.682	.443	.563
M5 M6	.761	.546	.654
M5 M7	.966	.148	.557
M5 M8	.705	.489	.597
M6 M7	.727	.466	.597
M6 M8	.841	.500	.641
M7 M8	.839	.534	.636
M1 M2 M3	.614	.750	.682
M1 M2 M4	.830	.614	.722
M1 M2 M5	.841	.534	.688
M1 M2 M6	.830	.534	.682
M1 M2 M7	.705	.534	.619
M1 M2 M8	.852	.534	.693
M1 M3 M4	.841	.500	.671
M1 M3 M5	.602	.705	.653
M1 M3 M6	.614	.659	.636
M1 M3 M7	.659	.557	.608
M1 M3 M8	.682	.614	.648
M1 M4 M5	.898	.500	.699
M1 M4 M6	.864	.534	.699
M1 M4 M7	.841	.432	.636
M1 M4 M8	.773	.398	.585
M1 M5 M6	.671	.681	.676
M1 M5 M7	.885	.546	.716
M1 M5 M8	.909	.455	.682
M1 M6 M7	.807	.477	.642
M1 M6 M8	.875	.443	.659
M1 M7 M8	.727	.534	.631
M2 M3 M4	.841	.500	.671
M2 M3 M5	.761	.636	.699
M2 M3 M6	.800	.568	.684
M2 M3 M7	.807	.602	.705

Feature Space	Liver Success Rate	Spleen Success Rate	Total Success Rate
M2 M3 M8	.659	.659	.659
M2 M4 M5	.807	.557	.682
M2 M4 M6	.886	.568	.727
M2 M4 M7	.886	.625	.756
M2 M4 M8	.830	.568	.699
M2 M5 M6	.818	.511	.665
M2 M5 M7	.841	.511	.676
M2 M5 M8	.796	.500	.648
M2 M6 M7	.898	.455	.676
M2 M6 M8	.830	.557	.693
M2 M7 M8	.761	.523	.642
M3 M4 M5	.898	.534	.716
M3 M4 M6	.864	.511	.688
M3 M4 M7	.852	.534	.693
M3 M4 M8	.773	.591	.682
M3 M5 M6	.716	.580	.648
M3 M5 M7	.886	.489	.688
M3 M5 M8	.705	.580	.642
M3 M6 M7	.852	.489	.671
M3 M6 M8	.727	.602	.655
M3 M7 M8	.614	.636	.625
M4 M5 M6	.886	.477	.682
M4 M5 M7	.977	.091	.534
M4 M5 M8	.841	.409	.625
M4 M6 M7	.943	.375	.659
M4 M6 M8	.864	.489	.676
M4 M7 M8	.830	.511	.671
M5 M6 M7	.886	.477	.682
M5 M6 M8	.886	.477	.682
M5 M7 M8	.886	.477	.682
M6 M7 M8	.886	.477	.682

BIBLIOGRAPHY

BIBLIOGRAPHY

1. P.P. Lele, and N. Senapati, "The Frequency Spectra of Energy Backscattered and Attenuated by Normal and Abnormal Tissue", Recent Advances in Ultrasound in Biomedicine, Volume 1, 1977, D.N. White, Editor.

2. F.L. Lizzi, M.A. Laviola, and D.J. Coleman, "Ultrasonic Tissue Characterization Using Spectrum Analysis", Proceedings of the Society of Photo-Optical Instrumentation Engineers, Volume 96, 1976.

3. F.L. Lizzi, and M.A. Laviola, "Tissue Signature Characterization Utilizing Frequency Domain Analysis", Ultrasonics Symposium Proceedings, 1976, IEEE Cat. #76 CH1120-5SU.

4. F.L. Lizzi, L. Katz, L. St. Louis, and D.J. Coleman, "Applications of Spectral Analysis in Medical Ultrasonography", Ultrasonics, March 1976.

5. J. Fraser, and G.S. Kino, "Cepstral Signal Processing for Tissue Signal Analysis", Second International Symposium on Ultrasonic Tissue Characterization, 1977.

6. W.K. Chu, and D.E. Raeside, "Fourier Analysis of the Echocardiogram", Phys. Med. Biol, Volume 23, No. 1, 100-105, 1978.

7. M.G. Czerwinski, D.E. Leb, and K. Preston, Jr., "Ultrasonic Characterization of Pyelomephritis in the Rabbit", Third International Symposium on Ultrasonic Imaging and Tissue Characterization, 1978.

8. P.M. Morse, and K.U. Ingard", Theoretical Acoustics", Internation Series in Pure and Applied Science, McGraw-Hill Book Company, 1968.

9. P.N.T. Wells, "Physical Principles of Ultrasonic Diagnosis", Academic Press, 1969.

10. Karl F. Herzfeld and Theodore A. Litovitz, "Absorption and Dispersion of Ultrasonic Waves", Academic Press, 1959.

11. Roman Kue, Mischa Schwartz, Nathaniel Finby, and Frank Dain, "Livertissue Characterization Using Reflected Ultrasonic Signals", Submitted for publication to IEEE Transactions on Biomedical Engineering.

12. S.A. Goss, R.C. Johnston, and F. Dunn, "Comprehensive Complication of Empirical Ultrasonic Propeties of Mammalian Tissue", J. Acoustic Association of America, 1978.

13. Mark Robert Funk, "A Digital Ultrasound System for Data Collection, Imaging, and Tissue Signature Analysis", Masters Thesis, Electrical Engineering and System Science, Michigan State University.

14. Phillip Chemento, Michigan State University. ULTRA documentation, Unpublished.

15. Goldberg and Watson, "Collision Theory", John Wiley, 1964.

16. J.C. Gore and S. Leeman, "Ultrasonic Backscattering from Human Tissue: A Realistic Model", Physical Medical Biology, 1977.

17. R.C. Wagg, R.M. Lerner and R. Gramak, "Swept - Frequency Ultrasonic Determination of Tissue Macrostructures", Proceedings of NSF - NBS Seminar on Tissue Characterization.

18. Duda and Hart, "Pattern Classification and Scene Analysis", Wiley Interscience, 1973.

19. N. Hassani, "Hepatic Sonography", Ultrasonography of the Abdomin, 1976.

20. N. Hassani, "Splenic Sonography", Ultrasonography of the Abdomin, 1976.